

# UC Irvine

## UC Irvine Previously Published Works

### Title

Complexes of HNO<sub>3</sub> and NO<sub>3</sub> - with NO<sub>2</sub> and N<sub>2</sub>O<sub>4</sub>, and their potential role in atmospheric HONO formation.

### Permalink

<https://escholarship.org/uc/item/7m30g6dz>

### Journal

Physical chemistry chemical physics : PCCP, 10(39)

### ISSN

1463-9076

### Authors

Kamboores, Michael A  
Raff, Jonathan D  
Miller, Yifat  
[et al.](#)

### Publication Date

2008-10-21

Peer reviewed

# Complexes of HNO<sub>3</sub> and NO<sub>3</sub><sup>−</sup> with NO<sub>2</sub> and N<sub>2</sub>O<sub>4</sub>, and their potential role in atmospheric HONO formation†

Michael A. Kamboures,<sup>a</sup> Jonathan D. Raff,<sup>a</sup> Yifat Miller,<sup>b</sup> Leon F. Phillips,<sup>c</sup> Barbara J. Finlayson-Pitts<sup>a</sup> and R. Benny Gerber<sup>\*ab</sup>

Received 31st March 2008, Accepted 21st July 2008

First published as an Advance Article on the web 11th August 2008

DOI: 10.1039/b805330h

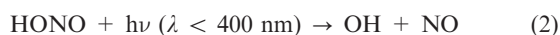
Calculations were performed to determine the structures, energetics, and spectroscopy of the atmospherically relevant complexes (HNO<sub>3</sub>)·(NO<sub>2</sub>), (HNO<sub>3</sub>)·(N<sub>2</sub>O<sub>4</sub>), (NO<sub>3</sub><sup>−</sup>)·(NO<sub>2</sub>), and (NO<sub>3</sub><sup>−</sup>)·(N<sub>2</sub>O<sub>4</sub>). The binding energies indicate that three of the four complexes are quite stable, with the most stable (NO<sub>3</sub><sup>−</sup>)·(N<sub>2</sub>O<sub>4</sub>) possessing binding energy of almost −14 kcal mol<sup>−1</sup>. Vibrational frequencies were calculated for use in detecting the complexes by infrared and Raman spectroscopy. An ATR-FTIR experiment showed features at 1632 and 1602 cm<sup>−1</sup> that are attributed to NO<sub>2</sub> complexed to NO<sub>3</sub><sup>−</sup> and HNO<sub>3</sub>, respectively. The electronic states of (HNO<sub>3</sub>)·(N<sub>2</sub>O<sub>4</sub>) and (NO<sub>3</sub><sup>−</sup>)·(N<sub>2</sub>O<sub>4</sub>) were investigated using an excited state method and it was determined that both complexes possess one low-lying excited state that is accessible through absorption of visible radiation. Evidence for the existence of (NO<sub>3</sub><sup>−</sup>)·(N<sub>2</sub>O<sub>4</sub>) was obtained from UV/vis absorption spectra of N<sub>2</sub>O<sub>4</sub> in concentrated HNO<sub>3</sub>, which show a band at 320 nm that is blue shifted by 20 nm relative to what is observed for N<sub>2</sub>O<sub>4</sub> dissolved in organic solvents. Finally, hydrogen transfer reactions within the (HNO<sub>3</sub>)·(NO<sub>2</sub>) and (HNO<sub>3</sub>)·(N<sub>2</sub>O<sub>4</sub>) complexes leading to the formation of HONO, were investigated. In both systems the calculated potential profiles rule out a thermal mechanism, but indicate the reaction could take place following the absorption of visible radiation. We propose that these complexes are potentially important in the thermal and photochemical production of HONO observed in previous laboratory and field studies.

## Introduction

Reactions in and on thin water films on surfaces are of intrinsic chemical interest because their kinetics and mechanisms may be quite different from those in the bulk aqueous or gas phase. For example, the hydrolysis of NO<sub>2</sub> is very slow in both phases, yet it is known to occur at a measurable rate in thin water films on surfaces:<sup>1</sup>



This reaction is potentially important in the lower atmosphere as a source of gaseous HONO, which has been shown by a number of studies to be a major photolytic source of the highly reactive OH free radical in continental regions.<sup>1–5</sup>



However, despite the importance of reaction (1), its mechanism is not well understood. In addition, both field<sup>3,4,6–8</sup> and laboratory

studies<sup>9–14</sup> suggest that there is also a photochemically driven source of HONO in that system. While a photoreduction of NO<sub>2</sub> involving organics such as phenols or humic acid has been suggested,<sup>12–14</sup> this would not explain the production of HONO when a glass manifold exposed to HNO<sub>3</sub> was irradiated in the absence of organics.<sup>10,15</sup> In addition, organics are not required for photochemical HONO production in environmental chambers.<sup>9,11,16–19</sup>

While many of these studies suggest that HNO<sub>3</sub> and/or NO<sub>3</sub><sup>−</sup> on surfaces are involved in the photochemistry, neither of these alone can explain the observations. HNO<sub>3</sub> has only a weak absorption tail in the actinic region above 290 nm that reaches Earth's surface,<sup>1</sup> and this generates NO<sub>2</sub> whose secondary thermal reactions to generate HONO are relatively slow. Although it had usually been assumed that HNO<sub>3</sub> formed during the NO<sub>2</sub> heterogeneous hydrolysis (reaction (1)) would dissociate to H<sup>+</sup> + NO<sub>3</sub><sup>−</sup>, laboratory studies<sup>20–22</sup> show this is not entirely the case. In fact, at 50% relative humidity, almost half of the surface-bound species is in the form of undissociated HNO<sub>3</sub> that is complexed to water or itself.<sup>22</sup> Donaldson and coworkers<sup>23</sup> showed that hydrates of HNO<sub>3</sub> have electronic states that are nearly identical to those of isolated HNO<sub>3</sub>, so that binding to water does not change the spectroscopy. Nitrate ions have a n → π\* transition that peaks at 310 nm, but this is also weak and decreases rapidly to negligible values at 340 nm.<sup>24,25</sup> In experiments performed in an environmental chamber (SAPHIR),<sup>26</sup> significant HONO production, up to 3 ppb h<sup>−1</sup>, continued when a filter that only transmitted light above 370 nm

<sup>a</sup> Department of Chemistry, University of California, Irvine, CA 92697, USA. E-mail: bgerber@uci.edu; Fax: +1 (1)972 2651 3742; Tel: +1 (1)972 2651 5732

<sup>b</sup> Department of Physical Chemistry and the Fritz Haber Research Center for Molecular Dynamics, Hebrew University, Jerusalem, 91904, Israel

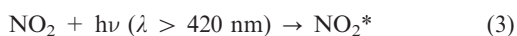
<sup>c</sup> Department of Chemistry, University of Canterbury, Private Bag 4800, Christchurch, New Zealand

† Electronic supplementary information (ESI) available: Vibrational frequencies, infrared intensities, and Raman intensities; additional configurations of (HONO)·(NO<sub>3</sub>). See DOI: 10.1039/b805330h

was used, suggesting that the chromophore(s) responsible must absorb beyond 370 nm, and ruling out both  $\text{HNO}_3$  and  $\text{NO}_3^-$  as the HONO precursor.

During the heterogeneous hydrolysis reaction (1),  $\text{NO}_2$  and/or  $\text{N}_2\text{O}_4$  must be taken up on the thin water film and it has been hypothesized<sup>27–29</sup> that a key step in the reaction is the isomerization of symmetric  $\text{O}_2\text{NNO}_2$  to asymmetric  $\text{ONONO}_2$ . Both  $\text{NO}_2$  and  $\text{N}_2\text{O}_4$  absorb light to 400 nm and beyond.<sup>1,30,31</sup> Thus, one possible explanation for the field and laboratory observations may be the formation of complexes between  $\text{NO}_2$  and/or  $\text{N}_2\text{O}_4$  and  $\text{HNO}_3$  or  $\text{NO}_3^-$  on surfaces. If the  $\text{NO}_2/\text{N}_2\text{O}_4$  imbued the complexes with their chromophoric properties, photochemistry may occur that results in HONO formation. Such complexes may also play a previously unrecognized role in the thermal reaction (1).

Little is known about the structure, stability or spectroscopy of these potential complexes. Barnes *et al.*<sup>32</sup> reported the formation of a complex of  $\text{NO}_2$  with  $\text{HNO}_3$  in argon matrices at a temperature of 5 K, and a similar complex was tentatively identified in thin water films exposed to gas phase  $\text{NO}_2$  at room temperature by Ramazan *et al.*<sup>22</sup> Indirect support for the involvement of  $\text{NO}_2/\text{N}_2\text{O}_4$  comes from the SAPHIR chamber experiments in which the photochemical production rate of HONO could be parameterized by a term involving the photolysis rate of  $\text{NO}_2$  in the chamber.<sup>16</sup> Li *et al.*<sup>33</sup> recently reported that electronically excited  $\text{NO}_2$ , generated by absorption beyond 420 nm, where dissociation to  $\text{NO} + \text{O}(^3\text{P})$  does not occur, reacts with water vapor to generate  $\text{OH} + \text{HONO}$ .



It seems unlikely that this is the source of HONO in the SAPHIR chamber experiments, as Rohrer *et al.*<sup>26</sup> ruled out photolysis primarily at  $\lambda > 420$  nm based on the results of the cutoff filter experiments. Also, evidence suggests that reactions (3) and (4) may not be as strong a gas-phase HONO source as Li *et al.* proposed.<sup>34,35</sup>

There are also two earlier reports of enhanced  $\text{HNO}_3$  photolysis in the presence of  $\text{NO}_2$  at wavelengths of 366 and 265 nm<sup>36,37</sup> under anhydrous conditions, although traces of water may have been present. The observed loss of  $\text{HNO}_3$  was eventually explained as being due to the heterogeneous reaction of  $\text{NO}$  with  $\text{HNO}_3$  on the surfaces of the experimental apparatus.<sup>38</sup> However, under the high  $\text{NO}_2/\text{N}_2\text{O}_4$  concentrations in those early experiments, it is possible that complexes between  $\text{NO}_2$  and/or  $\text{N}_2\text{O}_4$  and  $\text{HNO}_3$  may have also been present and played a role in the observed enhancement of  $\text{HNO}_3$  photolysis.

We have carried out theoretical and experimental studies of these complexes to assess their potential contribution to atmospheric heterogeneous chemistry. Specifically, we seek to: (1) identify the geometric structures and determine the stabilities of the complexes,  $(\text{HNO}_3)\cdot(\text{NO}_2)$ ,  $(\text{NO}_3^-)\cdot(\text{NO}_2)$ ,  $(\text{HNO}_3)\cdot(\text{N}_2\text{O}_4)$ , and  $(\text{NO}_3^-)\cdot(\text{N}_2\text{O}_4)$ ; (2) calculate their vibrational frequencies, infrared intensities, and Raman activities, for use in detecting these complexes in laboratory experiments; (3) identify whether or not these complexes are chromophores using an excited state method; (4) examine the possibility that

photochemically driven intramolecular hydrogen atom transfer reactions within the  $(\text{HNO}_3)\cdot(\text{NO}_2)$  and  $(\text{HNO}_3)\cdot(\text{N}_2\text{O}_4)$  complexes can lead to the formation of HONO; and (5) search for evidence of the complexes using infrared and UV/vis spectroscopy. While the results of the gas-phase calculations may not extrapolate quantitatively to conditions present on surfaces under atmospheric conditions, they can serve as a guide to determine if it is reasonable that such complexes play a role in atmospheric chemistry.

## Methods

### Computational details

The following electronic structure methods were used to determine the potential energies of chemical structures using the GAMESS suite of programs: (1) spin-restricted open-shell Hartree–Fock (ROHF)<sup>39</sup> (2) Becke-3-parameter exchange, Lee–Yang–Parr (B3LYP) correlation density functional theory,<sup>40–42</sup> and (3) spin-restricted open-shell Hartree–Fock with second order Møller–Plesset perturbation (ROMP2).<sup>43</sup> These methods were chosen for their ability to handle open-shell systems.

The GAMESS triple zeta valence basis set augmented with polarization functions on all atoms (TZP)<sup>44</sup> was used to model all molecular orbitals. This also accurately treated hydrogen bonding present in a number of the complexes investigated. The TZP basis set, along with MP2, was used recently by Miller *et al.*<sup>45</sup> to determine vibrational frequencies for similar H-bonded systems involving *cis*-HONO, *trans*-HONO,  $\text{HNO}_3$ ,  $(\text{HNO}_3)\cdot(\text{H}_2\text{O})$  and  $\text{HNO}_4$  that were in reasonable agreement with those obtained through experiments. Atomic charges were calculated using the Löwdin scheme in which the atomic orbitals and molecular orbital coefficients are converted to an orthogonal set generating electron populations that are less sensitive to basis set type.<sup>46</sup>

Electronic binding energies,  $D_0$ , were obtained for the complexes by taking the electronic potential energy of the optimized complex and subtracting from it the electronic potential energies of its subunits in their optimized isolated states. Zero point vibrational energy (ZPE) corrected binding energies,  $D_e$ , were obtained through a similar treatment. Corrections for basis set superposition errors (BSSE) were not made.

The electronic transitions of  $(\text{HNO}_3)\cdot(\text{N}_2\text{O}_4)$ ,  $(\text{NO}_3^-)\cdot(\text{N}_2\text{O}_4)$ , and  $\text{N}_2\text{O}_4$  were investigated using configuration interaction singles (CIS). All single substitutions of the ground state ROMP2/TZP spin orbitals by virtual orbitals were allowed. The wavefunction of the lowest energy excited electronic state of each chemical species was obtained. Vertical excitation energies to these states from their corresponding ground states, and the integrated intensities for these transitions (oscillator strengths) were computed. The  $\lambda_{\text{max}}$  absorption cross-section  $\sigma_A$  for transitions in the complexes were estimated from the ratios of the calculated integrated intensities, the absorption frequencies, and the experimental value of the absorption cross section for  $\text{N}_2\text{O}_4$ <sup>31</sup> with the assumption that the line shapes for the transitions in the complexes were identical to that of isolated  $\text{N}_2\text{O}_4$ .<sup>47</sup>

The CIS method generally overestimates excitation energies.<sup>48–50</sup> However, the method can be used to estimate shifts in the vertical excitation frequency of a chromophore due to changes in its chemical environment due to complexation and solvation.<sup>23,49,51,52</sup> In this study we calculated the absolute CIS vertical excitation energies of  $(\text{HNO}_3)\cdot(\text{N}_2\text{O}_4)$  and  $(\text{NO}_3^-)\cdot(\text{N}_2\text{O}_4)$  and corrected them by subtracting the difference between the calculated and experimental vertical excitation frequencies of isolated  $\text{N}_2\text{O}_4$ .<sup>31,53</sup>

Vibrational frequencies, infrared intensities, and Raman intensities were determined for all ROMP2-derived structures using the appropriate functions in GAMESS.<sup>54–56</sup> Vibrational frequencies calculated using the harmonic approximation may deviate from the experimental values. More accurate estimates of experimental vibrational frequencies of the complexes were obtained by applying the correction:

$$\nu_{\text{exp}}^{\text{complex}} = \nu_{\text{calc}}^{\text{complex}} + \Delta\nu_{\text{subunit}} \quad (5)$$

where  $\nu_{\text{exp}}^{\text{complex}}$  is the predicted experimental frequency of a particular mode,  $\nu_{\text{calc}}^{\text{complex}}$  is the uncorrected computed frequency, and  $\Delta\nu_{\text{subunit}}$  is the difference (shift) between the computed and experimental frequency of the subunit taken from literature.

### Infrared spectroscopy of surfaces exposed to $\text{HNO}_3$ and $\text{NO}_x$

IR spectra were collected using a Thermo Nicolet Avatar 370 Fourier transform infrared spectrometer equipped with an attenuated total reflection (ATR) probe (Axiom Analytical). The internal reflection element (IRE) installed at the end of the probe was either an AMTIR ( $\text{Ge}_{33}\text{As}_{12}\text{Se}_{55}$ ) or silicon (Si) rod, 0.6 cm dia.  $\times$  4 cm long with 45° conical ends. The surface of the AMTIR rod was coated with a 20 nm thick (measured by ellipsometry) layer of  $\text{SiO}_x$  using plasma-enhanced chemical vapor deposition. The probe was cleaned between experiments by rinsing with water (Millipore, 18.2 M $\Omega$  cm) to remove adsorbed nitrate species. The spectrometer casing and interior of the ATR probe were purged with nitrogen to eliminate spectral interferences from water vapor and  $\text{CO}_2$  in ambient air.

In a typical experiment, the ATR probe was inserted into a vacuum-tight borosilicate glass reaction chamber (1.75 L) and evacuated for 1–2 days at  $\sim 10^{-4}$  Torr. Surfaces in the reaction chamber were conditioned by repeated exposure to  $\sim 20$  Torr of  $\text{NO}_2\text{--N}_2\text{O}_4$ , followed by evacuation for 1 h at  $\sim 10^{-4}$  Torr. The IRE was then exposed to anhydrous  $\text{HNO}_3$  for 1 h before introducing a mixture of  $\text{NO}_2\text{--N}_2\text{O}_4$  from the attached vacuum line. Single beam spectra were recorded under vacuum and then in the presence of mixtures of  $\text{HNO}_3$ ,  $\text{NO}_2$  and  $\text{N}_2\text{O}_4$  at  $295 \pm 1$  K. Infrared spectra were averages of 1000 scans recorded at a resolution of 2  $\text{cm}^{-1}$ .

$\text{NO}_2$  was synthesized from the reaction of NO (Matheson, 99%) with excess oxygen (Oxygen Service Company, 99.993%), followed by trap-to-trap purification. Nitric oxide was purified by passing it through an acetone–dry ice bath trap at 195 K before use. Anhydrous  $\text{HNO}_3$  was obtained from the vapor above a 1 : 2 v/v solution of  $\text{HNO}_3$  (70 wt%  $\text{HNO}_3$ , 99.999+%, Sigma-Aldrich) and  $\text{H}_2\text{SO}_4$  (>95 wt%, Fluka).

### Ultraviolet/visible spectroscopy of $\text{N}_2\text{O}_4$ solutions

Solutions of  $\text{N}_2\text{O}_4$  in  $\text{HNO}_3$  were prepared by trapping  $\text{NO}_2$  (1% w/w) in a Schlenk flask containing concentrated  $\text{HNO}_3$  under vacuum at 78 K, followed by warming to room temperature. The UV/vis absorption spectra of solutions of  $\text{HNO}_3\text{--N}_2\text{O}_4$  and  $\text{N}_2\text{O}_4$ -free concentrated  $\text{HNO}_3$  were obtained by adding a drop of either solution between two quartz microscope slides placed into a light path of the spectrophotometer. The solution of  $\text{N}_2\text{O}_4$  in acetonitrile was prepared by adding tetrabutylammonium nitrate to excess nitrosonium tetrafluoroborate ( $\text{NOBF}_4$ ) dissolved in anhydrous acetonitrile, in a glove bag under an atmosphere of dry  $\text{N}_2$ . Spectra of this solution were obtained in a quartz cell with a 0.1 mm pathlength.

All spectra were obtained at room temperature using an Ocean Optics HR4000 spectrophotometer.  $\text{NOBF}_4$  (95%), tetrabutylammonium nitrate (97%), and anhydrous acetonitrile (99.8%) were from Sigma-Aldrich and used without further purification.

## Results and discussion

### $\text{NO}_x$ complexes: structures and stabilities

Minimum energy structures of the binary complexes,  $(\text{HNO}_3)\cdot(\text{NO}_2)$ ,  $(\text{HNO}_3)\cdot(\text{N}_2\text{O}_4)$ ,  $(\text{NO}_3^-)\cdot(\text{NO}_2)$  and  $(\text{NO}_3^-)\cdot(\text{N}_2\text{O}_4)$  were located using ROHF, ROMP2, and B3LYP. Each method located one minimum for each complex. The binding energies for the four binary chemical complexes with and without zero-point energy (ZPE) corrections are shown in Table 1. Results indicate that the two complexes containing  $\text{N}_2\text{O}_4$  possess substantially larger binding energies than the two complexes containing  $\text{NO}_2$ . In addition, the two complexes which contain  $\text{NO}_3^-$  have significantly greater binding energies than the two complexes that contain  $\text{HNO}_3$ . The structures and the stabilities for each of the four complexes are discussed below. It should be noted that the calculations presented here are all for the gas phase species. The substrate may have some impact on the calculated energetics of the complexes and the subunits, but this cannot be taken into account until there are data available on the nature of the interactions with the surface.

### $(\text{HNO}_3)\cdot(\text{NO}_2)$

The ROMP2 optimized minimum energy structure for  $(\text{HNO}_3)\cdot(\text{NO}_2)$  is planar and the orientation of the O–H bond of  $\text{HNO}_3$  is toward an oxygen atom of  $\text{NO}_2$  (Fig. 1a). Bond angle and distance criteria<sup>57,58</sup> indicate that a hydrogen bond exists between O(3)–H $\cdots$ O(6). Similar results were obtained using the ROHF and B3LYP methods. The ZPE-corrected binding energies for  $(\text{HNO}_3)\cdot(\text{NO}_2)$  are between  $-2.4$  and  $-2.8$   $\text{kcal mol}^{-1}$ , depending upon the method (Table 1). These are weak compared to the binding energies reported for the nitric acid–water complex which are in the range of 7–10  $\text{kcal mol}^{-1}$ .<sup>23,59,60</sup> Assuming similar entropy changes upon complex formation, the enthalpy differences result in the equilibrium constant for complex formation with  $\text{H}_2\text{O}$  being larger than that for complex formation with  $\text{NO}_2$  by at least a factor of  $10^2$  at 300 K.

**Table 1** Binding energies of the complexes before ( $D_0$ ) and after ( $D_e$ ) the zero-point energy correction

Complex	ROHF/TZP		ROMP2/TZP		B3LYP/TZP	
	$D_0/\text{kcal mol}^{-1}$	$D_e/\text{kcal mol}^{-1}$	$D_0/\text{kcal mol}^{-1}$	$D_e/\text{kcal mol}^{-1}$	$D_0/\text{kcal mol}^{-1}$	$D_e/\text{kcal mol}^{-1}$
(HNO <sub>3</sub> )·(NO <sub>2</sub> )	-3.7	-2.8	-3.3	-2.4	-3.3	-2.5
(NO <sub>3</sub> <sup>-</sup> )·(NO <sub>2</sub> )	-4.6	-3.9	-3.9	-3.1	-6.0	-5.5
(HNO <sub>3</sub> )·(N <sub>2</sub> O <sub>4</sub> )	-7.8	-7.0	-8.2	-7.3	-6.0	-5.5
(NO <sub>3</sub> <sup>-</sup> )·(N <sub>2</sub> O <sub>4</sub> )	-14.0	-13.1	-13.1	-12.2	-14.6	-14.0

The structure is nearly identical to the B3LYP/6-31G(d,p) structure for (HNO<sub>3</sub>)·(NO<sub>2</sub>) reported by Dimitrova and Peyerimhoff,<sup>61</sup> who reported an MP2/6-311+G\*\* binding energy for (HNO<sub>3</sub>)·(NO<sub>2</sub>) of  $-4.4 \text{ kcal mol}^{-1}$ , without correcting for ZPE.

### (HNO<sub>3</sub>)·(N<sub>2</sub>O<sub>4</sub>)

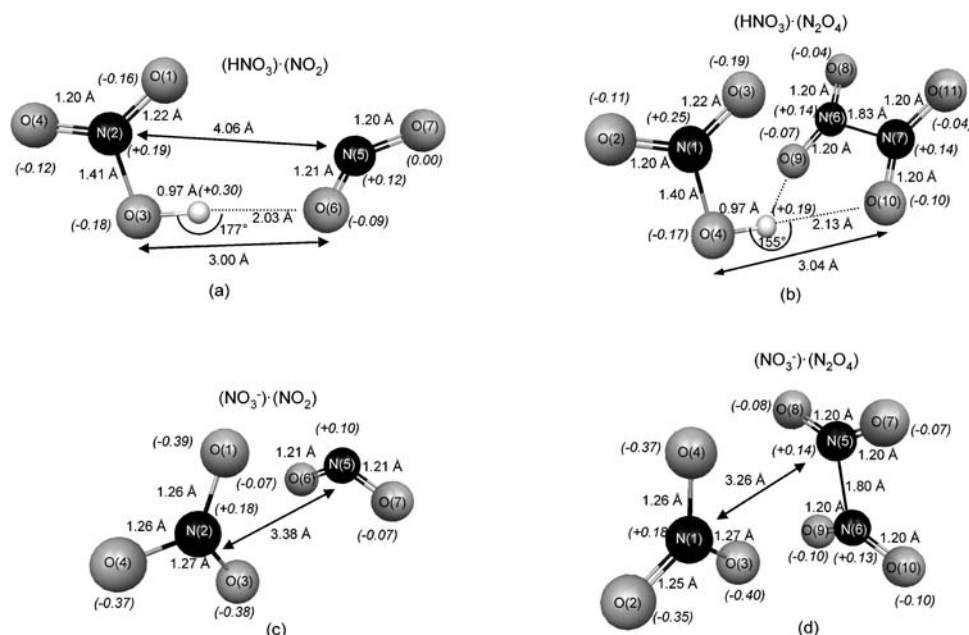
The ROMP2 optimized structure for (HNO<sub>3</sub>)·(N<sub>2</sub>O<sub>4</sub>) is shown in Fig. 1b. Similar to (HNO<sub>3</sub>)·(NO<sub>2</sub>), the O–H bond of HNO<sub>3</sub> is oriented towards the two O atoms of N<sub>2</sub>O<sub>4</sub> in the complex and is involved in hydrogen bonding. The four remaining atoms of N<sub>2</sub>O<sub>4</sub> tilt away from the HNO<sub>3</sub> subunit. The internal coordinates of HNO<sub>3</sub> and N<sub>2</sub>O<sub>4</sub> are not substantially distorted by complexation. The ROMP2 structure of (HNO<sub>3</sub>)·(N<sub>2</sub>O<sub>4</sub>) is very similar to the corresponding ROHF and B3LYP structures, although the N–N bond length in the N<sub>2</sub>O<sub>4</sub> subunit is approximately 0.20 Å shorter than in the ROMP2 and B3LYP structures. A similar difference is observed in the N–N bond length of isolated N<sub>2</sub>O<sub>4</sub> using ROHF *versus* the other two methods. We suggest that this may be due to the incorrect assignment of local molecular orbital energies because of the absence of correlation in the ROHF Hamiltonian.

Table 1 shows that the calculated binding energies for (HNO<sub>3</sub>)·(N<sub>2</sub>O<sub>4</sub>) are more than twice as large as corresponding

binding energies for (HNO<sub>3</sub>)·(NO<sub>2</sub>). While there is one hydrogen bond in the (HNO<sub>3</sub>)·(N<sub>2</sub>O<sub>4</sub>), the stronger binding energy relative to (HNO<sub>3</sub>)·(NO<sub>2</sub>) arises from the strong dipole-induced dipole interaction between N<sub>2</sub>O<sub>4</sub> and HNO<sub>3</sub> in the complex. The experimental polarizability of N<sub>2</sub>O<sub>4</sub> is double that of NO<sub>2</sub><sup>62–64</sup> and is more susceptible to charge distortion near polar molecules like HNO<sub>3</sub>. The Löwdin charges calculated here also confirm that N<sub>2</sub>O<sub>4</sub> is polarized by HNO<sub>3</sub> in the complex through a dipole-induced dipole effect.

### (NO<sub>3</sub><sup>-</sup>)·(NO<sub>2</sub>)

Fig. 1c shows the ROMP2 optimized structure of (NO<sub>3</sub><sup>-</sup>)·(NO<sub>2</sub>). The ROMP2, ROHF and B3LYP structures for this complex are very similar. In general, nitrogen atoms of NO<sub>3</sub><sup>-</sup> and NO<sub>2</sub> are separated in the complex by a relatively short distance, 3.27–3.38 Å, depending upon the method. The NO<sub>3</sub><sup>-</sup> subunit remains planar in the complex. The N–O bond lengths of NO<sub>3</sub><sup>-</sup> remain nearly equivalent to one another in (NO<sub>3</sub><sup>-</sup>)·(NO<sub>2</sub>). The sums of the atomic charges for NO<sub>3</sub><sup>-</sup> and NO<sub>2</sub> in the complex were always near  $-1.0$  and  $0.0$ , respectively, suggesting that NO<sub>3</sub><sup>-</sup> remains a closed-shell anion when complexed to NO<sub>2</sub>. Table 1 shows the ZPE-corrected binding energies for (NO<sub>3</sub><sup>-</sup>)·(NO<sub>2</sub>) which are larger than those obtained for (HNO<sub>3</sub>)·(NO<sub>2</sub>) by all three methods.



**Fig. 1** The ROMP2/TZP optimized structures of (a) (HNO<sub>3</sub>)·(NO<sub>2</sub>), (b) (HNO<sub>3</sub>)·(N<sub>2</sub>O<sub>4</sub>), (c) (NO<sub>3</sub><sup>-</sup>)·(NO<sub>2</sub>), and (d) (NO<sub>3</sub><sup>-</sup>)·(N<sub>2</sub>O<sub>4</sub>). Löwdin atomic charges are listed adjacent to the atoms in parentheses.

**(NO<sub>3</sub><sup>-</sup>)(N<sub>2</sub>O<sub>4</sub>)**

The ROMP2-optimized structure of (NO<sub>3</sub><sup>-</sup>)(N<sub>2</sub>O<sub>4</sub>) is shown in Fig. 1d. Calculations indicate that the binding of NO<sub>3</sub><sup>-</sup> to N<sub>2</sub>O<sub>4</sub> is a very exoergic process with computed binding energies that are about twice as large as those calculated for the next most stable complex, (HNO<sub>3</sub>)(N<sub>2</sub>O<sub>4</sub>); Table 1. The strong interaction is attributed to an ion-induced dipole effect. The large polarizability of N<sub>2</sub>O<sub>4</sub> relative to NO<sub>2</sub> makes N<sub>2</sub>O<sub>4</sub> more susceptible to induction *via* the electric field of NO<sub>3</sub><sup>-</sup>, causing the N<sub>2</sub>O<sub>4</sub> subunit to be polarized along the axis of the N–N bond.

**Calculated vibrational frequencies of the NO<sub>x</sub> complexes**

Detecting NO<sub>x</sub> complexes based on their Raman shifts or infrared absorption bands is complicated due to interferences between vibrational features of the complexes and the subunits making up the complexes. Infrared absorption intensities, Raman activities, vibrational frequencies, and vibrational frequency shifts due to complexation for the four complexes were calculated to aid in identifying these complexes in laboratory experiments. Emphasis is placed on identifying the vibrational modes of the complexes whose frequencies are shifted from their corresponding values in the uncomplexed molecules. The calculated and experimentally determined frequencies of the uncomplexed molecules are tabulated in the ESI† and will not be discussed in detail here since a number of high level modeling studies have been reported for the molecular vibrations of N<sub>2</sub>O<sub>4</sub>,<sup>28,65–72</sup> HNO<sub>3</sub>,<sup>45,64,73–75</sup> and NO<sub>2</sub>.<sup>76,77</sup>

The calculated spectroscopic results for (HNO<sub>3</sub>)(NO<sub>2</sub>) are given in Table 2. Rows corresponding to modes that may be identified by infrared and/or Raman spectroscopy are highlighted in boldface and italics, respectively. The last six modes listed for (HNO<sub>3</sub>)(NO<sub>2</sub>) are intermolecular modes whose atomic motions tend to involve atoms on both subunits.

Modes 1–12 correspond to vibrations that are intramolecular modes involving atoms on only one subunit.

Mode 1 of (HNO<sub>3</sub>)(NO<sub>2</sub>) corresponds to O–H stretching in the HNO<sub>3</sub> subunit. It has a computed band at 3714 cm<sup>-1</sup> that is shifted -70 cm<sup>-1</sup> and is ~5 times stronger than the corresponding band calculated for isolated HNO<sub>3</sub>. The utility of this mode in experimental studies will most likely depend upon the presence of water which has vibrational frequencies near 3400 cm<sup>-1</sup>.<sup>78</sup> Other potentially useful vibrational modes include the Raman-active ONO bend in the NO<sub>2</sub> subunit (mode 8) and mode 12 corresponding to HONO torsion in the HNO<sub>3</sub> subunit, which should be detectable with IR spectroscopy.

Dimitrova<sup>79</sup> used several theoretical methods along with a scaling procedure to calculate predicted experimental frequencies and frequency shifts for (HNO<sub>3</sub>)(NO<sub>2</sub>). The average percent deviation between our ROMP2/TZP predicted experimental frequencies and those computed by Dimitrova's best method (B3LYP/6-31G(d,p)) was 3.6%. For vibrational modes in which our ROMP2/TZP and Dimitrova's B3LYP/6-31G(d,p) calculations both predict non-zero frequency shifts, the direction of the shift is the same in nine out of ten cases.

Finally, Barnes *et al.*<sup>32</sup> have reported the infrared spectrum of (HNO<sub>3</sub>)(NO<sub>2</sub>) in an argon matrix. They assigned two bands to the O–H stretching and HONO torsion vibrations of HNO<sub>3</sub> and one band to the asymmetric stretching mode of NO<sub>2</sub>. Our ROMP2/TZP predicted experimental frequencies for these three modes are in good agreement with the measured peak frequencies of Barnes, deviating by an average of only 3.3%. Dimitrova's B3LYP/6-31G(d,p) predicted frequencies were also in good agreement with Barnes' frequencies, deviating by an average of 3.8%.

The vibrational frequencies for (HNO<sub>3</sub>)(N<sub>2</sub>O<sub>4</sub>) are presented in Table 3. Mode 6 of (HNO<sub>3</sub>)(N<sub>2</sub>O<sub>4</sub>) is due to HON bending in the HNO<sub>3</sub> subunit and is a good candidate for identification

**Table 2** Vibrational frequencies, infrared intensities, and Raman intensities for (HNO<sub>3</sub>)(NO<sub>2</sub>) obtained using ROMP2/TZP

(HNO <sub>3</sub> )(NO <sub>2</sub> )		Frequencies			Calculated intensities	
Mode	Description	Calculated/cm <sup>-1</sup>	Shift <sup>a</sup> /cm <sup>-1</sup>	Predicted <sup>a</sup> experimental/cm <sup>-1</sup>	Infrared/km mol <sup>-1</sup>	Raman/Å <sup>4</sup> amu <sup>-1</sup>
<b>1</b>	<b><i>OH stretch of HNO<sub>3</sub></i></b>	<b><i>3714</i></b>	<b><i>-70</i></b>	<b><i>3422</i></b>	<b><i>440</i></b>	<b><i>49</i></b>
2	ONO asymmetric stretch of HNO <sub>3</sub>	1853	-11	1687	190	20
3	ONO asymmetric stretch of NO <sub>2</sub>	1844	0	1618	400	240
<b>4</b>	<b><i>HON bend of HNO<sub>3</sub></i></b>	<b><i>1395</i></b>	<b><i>+44</i></b>	<b><i>1390</i></b>	<b><i>99</i></b>	<b><i>7.1</i></b>
5	ONO asymmetric stretch of NO <sub>2</sub>	1340	+18	1336	6.1	740
6	ONO asymmetric stretch of HNO <sub>3</sub>	1319	+5	1317	240	17
7	(H)ON stretch of HNO <sub>3</sub>	912	+17	920	210	12
8	<b><i>ONO bend of NO<sub>2</sub></i></b>	<b><i>802</i></b>	<b><i>+29</i></b>	<b><i>779</i></b>	<b><i>18</i></b>	<b><i>720</i></b>
9	OOON torsion of HNO <sub>3</sub>	765	+5	773	4.1	0.8
10	ONO bend of HNO <sub>3</sub>	677	+16	680	130	7.6
11	(H)ONO bend of HNO <sub>3</sub>	609	+17	615	7.9	4.6
<b>12</b>	<b><i>HONO torsion of HNO<sub>3</sub></i></b>	<b><i>599</i></b>	<b><i>+140</i></b>	<b><i>619</i></b>	<b><i>110</i></b>	<b><i>1.4</i></b>
13	Intermolecular	114	N.A.	114	5.0	1.0
14	Intermolecular	98	N.A.	98	0.68	2.5
15	Intermolecular	83	N.A.	83	1.1	1.8
16	Intermolecular	57	N.A.	57	0.81	4.4
17	Intermolecular	27	N.A.	27	0.41	1.6
18	Intermolecular	26	N.A.	26	0.83	1.5

<sup>a</sup> A scaling procedure was used to obtain more accurate calculated vibrational frequencies for the modes of the complexes. To do this, a frequency shift for each mode was obtained. The frequency shift is the difference between the computed frequency of the mode in the complex and the computed frequency of the corresponding mode in the isolated subunit. The shift is then added to the experimental derived frequency of the corresponding mode (taken from the literature) to generate a predicted experimental frequency for the vibrational mode in the complex.

**Table 3** Vibrational frequencies, infrared intensities, and Raman intensities for (HNO<sub>3</sub>)·(N<sub>2</sub>O<sub>4</sub>) obtained using ROMP2/TZP

(HNO <sub>3</sub> )·(N <sub>2</sub> O <sub>4</sub> )		Frequencies			Calculated intensities	
Mode	Description	Calculated/ cm <sup>-1</sup>	Shift <sup>a</sup> / cm <sup>-1</sup>	Predicted <sup>a</sup> experimental/ cm <sup>-1</sup>	Infrared/ km mol <sup>-1</sup>	Raman/ Å <sup>4</sup> amu <sup>-1</sup>
<b>1</b>	<b>OH stretch of HNO<sub>3</sub></b>	<b>3719</b>	<b>-65</b>	<b>3427</b>	<b>280</b>	<b>83</b>
2	In phase ONO asymmetric stretch of N <sub>2</sub> O <sub>4</sub>	1957	+10	1728	280	5.0
3	180° Out of phase ONO asymmetric stretch of N <sub>2</sub> O <sub>4</sub>	1916	-1	1717	50	34
4	ONO asymmetric stretch of HNO <sub>3</sub>	1844	-20	1678	350	11
5	In phase ONO asymmetric stretch of N <sub>2</sub> O <sub>4</sub>	1409	+4	1387	5.4	12
<b>6</b>	<b>HON bend of HNO<sub>3</sub></b>	<b>1401</b>	<b>+50</b>	<b>1396</b>	<b>81</b>	<b>4.6</b>
7	ONO symmetric stretch of HNO <sub>3</sub>	1322	+8	1320	210	28
8	180° Out of phase symmetric stretch of N <sub>2</sub> O <sub>4</sub>	1274	+4	1265	410	0.67
9	(H)ON stretch of HNO <sub>3</sub>	921	+26	929	170	8.0
10	In phase ONO bend of N <sub>2</sub> O <sub>4</sub>	833	+4	817	1.7	14
11	OOON torsion of HNO <sub>3</sub>	767	+7	775	2.5	0.12
12	180° Out of phase ONO bend of N <sub>2</sub> O <sub>4</sub>	761	+11	762	280	0.11
13	ONO bend of HNO <sub>3</sub>	682	+21	685	9.4	5.3
14	NOON torsion of N <sub>2</sub> O <sub>4</sub>	642	+5	662	0.050	0.40
15	(H)ONO bend of HNO <sub>3</sub>	613	+21	619	5.5	4.6
<b>16</b>	<b>HONO torsion of HNO<sub>3</sub></b>	<b>508</b>	<b>+49</b>	<b>528</b>	<b>26</b>	<b>0.70</b>
17	In phase ONN bend of N <sub>2</sub> O <sub>4</sub>	478	+8	488	0.51	20
18	OOON torsion of N <sub>2</sub> O <sub>4</sub>	405	+5	430	9.7	0.2
19	NN stretch of N <sub>2</sub> O <sub>4</sub>	266	+9	271	0.021	37
20	ONN bend of N <sub>2</sub> O <sub>4</sub>	214	+12	277	0.38	1.7
21	Intermolecular	124	N.A.	124	0.15	0.4
22	Intermolecular	121	N.A.	121	3.1	0.9
23	Intermolecular	100	N.A.	100	2.4	2.1
24	ONNO torsion of N <sub>2</sub> O <sub>4</sub>	72	-20	62	0.099	0.7
25	Intermolecular	56	N.A.	56	0.069	1.7
26	Intermolecular	41	N.A.	41	0.99	3.7
27	Intermolecular	24	N.A.	24	1.0	6.1

<sup>a</sup> For explanation of how shift and predicted experimental frequency were calculated see Table 2 footnote.

using IR, although it may be obscured by the asymmetric NO<sub>2</sub> stretch of the NO<sub>3</sub><sup>-</sup> ion at 1356 cm<sup>-1</sup>, which tends to be very broad.<sup>80</sup> Mode 1 of (HNO<sub>3</sub>)·(N<sub>2</sub>O<sub>4</sub>), corresponding to the O–H stretch of the HNO<sub>3</sub> subunit, should be detectable by both IR and Raman spectroscopy at 3427 cm<sup>-1</sup>, although the presence of water could preclude its detection. The increased intensity and red shift clearly indicates hydrogen bonding.<sup>58</sup>

Vibrational data for (NO<sub>3</sub><sup>-</sup>)·(NO<sub>2</sub>) are presented in Table 4. This complex does not possess unique vibrational modes that

could be used to identify it on surfaces. However, modes 2 and 3 of (NO<sub>3</sub><sup>-</sup>)·(NO<sub>2</sub>), which correspond to degenerate asymmetric stretching in the NO<sub>3</sub><sup>-</sup> subunit, could be suitable markers for measuring (NO<sub>3</sub><sup>-</sup>)·(NO<sub>2</sub>) in a molecular beam experiment where peaks are narrower.

Data for (NO<sub>3</sub><sup>-</sup>)·(N<sub>2</sub>O<sub>4</sub>) are presented in Table 5. Mode 15, which is due to the OOON torsion in the N<sub>2</sub>O<sub>4</sub> subunit, and the in-phase symmetric stretch in the N<sub>2</sub>O<sub>4</sub> subunit (mode 5), may be useful to detect (NO<sub>3</sub><sup>-</sup>)·(N<sub>2</sub>O<sub>4</sub>) using IR spectroscopy.

**Table 4** Vibrational frequencies, infrared intensities, and Raman intensities for (NO<sub>3</sub><sup>-</sup>)·(NO<sub>2</sub>) obtained using ROMP2/TZP

(NO <sub>3</sub> <sup>-</sup> )·(NO <sub>2</sub> )		Frequencies			Calculated intensities	
Mode	Description	Calculated/cm <sup>-1</sup>	Shift <sup>a</sup> /cm <sup>-1</sup>	Predicted <sup>a</sup> experimental/cm <sup>-1</sup>	Infrared/km mol <sup>-1</sup>	Raman/Å <sup>4</sup> amu <sup>-1</sup>
1	ONO asymmetric stretch of NO <sub>2</sub>	1855	+11	1629	240	20
2	NO <sub>3</sub> <sup>-</sup> asymmetric stretch of NO <sub>3</sub> <sup>-</sup>	1510	+17	1373	630	12
3	NO <sub>3</sub> <sup>-</sup> asymmetric stretch of NO <sub>3</sub> <sup>-</sup>	1477	-16	1340	570	5.2
4	ONO symmetric stretch of NO <sub>2</sub>	1335	+13	1331	4.1	1.4
5	NO <sub>3</sub> <sup>-</sup> symmetric stretch of NO <sub>3</sub> <sup>-</sup>	1067	+1	1051	0.43	47
6	OOON torsion of NO <sub>3</sub> <sup>-</sup>	830	-3	828	8.0	0.1
7	ONO bend of NO <sub>2</sub>	773	+1	751	2.6	1.4
8	ONO bend of NO <sub>3</sub> <sup>-</sup>	728	+2	722	14	5.3
9	ONO bend of NO <sub>3</sub> <sup>-</sup>	728	+2	722	0.65	4.2
10	Intermolecular	159	N.A.	159	6.3	4.5
11	Intermolecular	101	N.A.	101	0.43	7.8
12	Intermolecular	84	N.A.	84	7.7	0.2
13	Intermolecular	68	N.A.	68	1.4	0.1
14	Intermolecular	50	N.A.	50	0.042	3.5
15	Intermolecular	16	N.A.	16	0.19	0.3

<sup>a</sup> For explanation of how shift and predicted experimental frequency were calculated see Table 2 footnote.

**Table 5** Vibrational frequencies, infrared intensities, and Raman intensities for  $(\text{NO}_3^-)\cdot(\text{N}_2\text{O}_4)$  obtained using ROMP2/TZP

$(\text{NO}_3^-)\cdot(\text{N}_2\text{O}_4)$		Frequencies			Calculated intensities	
Mode	Description	Calculated/ $\text{cm}^{-1}$	Shift/ $\text{cm}^{-1}$	Predicted experimental/ $\text{cm}^{-1}$	Infrared/ $\text{km mol}^{-1}$	Raman/ $\text{\AA}^4 \text{amu}^{-1}$
1	In phase ONO asymmetric stretch of $\text{N}_2\text{O}_4$	1962	+15	1776	260	3.1
2	$180^\circ$ out of phase ONO asymmetric stretch of $\text{N}_2\text{O}_4$	1906	-11	1707	78	17
<b>3</b>	<b>Asymmetric stretch of <math>\text{NO}_3^-</math></b>	<b>1536</b>	<b>+43</b>	<b>1399</b>	<b>590</b>	<b>4.3</b>
<b>4</b>	<b>Asymmetric stretch of <math>\text{NO}_3^-</math></b>	<b>1462</b>	<b>-31</b>	<b>1325</b>	<b>630</b>	<b>4.2</b>
<b>5</b>	<b>In phase ONO symmetric stretch of <math>\text{N}_2\text{O}_4</math></b>	<b>1408</b>	<b>+3</b>	<b>1389</b>	<b>35</b>	<b>13</b>
6	$180^\circ$ out of phase symmetric stretch of $\text{N}_2\text{O}_4$	1280	+10	1271	300	1.5
7	Symmetric stretch of $\text{NO}_3^-$	1072	+6	1072 <sup>a</sup>	3.7	11
8	In phase ONO bend of $\text{N}_2\text{O}_4$	836	+7	820	3.0	25
9	OOON torsion of $\text{NO}_3^-$	828	-1	828 <sup>a</sup>	8.3	0.32
10	$180^\circ$ out of phase ONO bend of $\text{N}_2\text{O}_4$	763	+13	764	200	1.1
11	ONO bend of $\text{NO}_3^-$	731	+5	731 <sup>a</sup>	3.4	16
12	ONO bend of $\text{NO}_3^-$	728	+2	728 <sup>a</sup>	4.2	33
13	NOON torsion of $\text{N}_2\text{O}_4$	637	<b>0</b>	<b>657</b>	0.57	6.7
14	In phase ONN bend of $\text{N}_2\text{O}_4$	496	+26	506	0.13	5.5
<b>15</b>	<b>OOON torsion of <math>\text{N}_2\text{O}_4</math></b>	<b>443</b>	<b>+43</b>	<b>468</b>	<b>31</b>	<b>2.6</b>
16	NN stretch of $\text{N}_2\text{O}_4$	277	+20	282	1.2	26
17	ONN bend of $\text{N}_2\text{O}_4$	227	+25	290	0.0055	0.21
<b>18</b>	<b>Intermolecular</b>	<b>131</b>	<b>N.A.</b>	<b>131</b>	<b>14</b>	<b>0.73</b>
19	ONNO torsion of $\text{N}_2\text{O}_4$	125	+33	115	0.59	0.39
20	Intermolecular	102	N.A.	102	1.1	5.0
21	Intermolecular	84	N.A.	84	1.4	3.4
22	Intermolecular	63	N.A.	63	0.42	9.5
23	Intermolecular	37	N.A.	37	0/011	2.1
24	Intermolecular	14	N.A.	14	0.31	6.7

<sup>a</sup> For explanation of how shift and predicted experimental frequency were calculated see Table 2 footnote.

### Electronic spectroscopy of $\text{N}_2\text{O}_4$ complexes

Electronic transitions of  $(\text{HNO}_3)\cdot(\text{N}_2\text{O}_4)$ ,  $(\text{NO}_3^-)\cdot(\text{N}_2\text{O}_4)$ , and  $\text{N}_2\text{O}_4$  were explored using configuration interaction singles (CIS) to identify to what extent the complexes absorb visible radiation. If they absorb visible light strongly then the photoactivation of these complexes *via* solar radiation might lead to chemistry that generates HONO or other volatile nitrogen oxides on urban surfaces.

When the CIS method was applied to isolated  $\text{N}_2\text{O}_4$ , the computed energy difference between the ground and first excited electronic states of the molecule was computed to be 4.38 eV (283 nm). The experimental gas-phase spectrum of  $\text{N}_2\text{O}_4$  has a strong absorption band centered at 340 nm (3.65 eV). Therefore, the CIS approach overestimates the energy for the transition in isolated  $\text{N}_2\text{O}_4$  by 0.73 eV.<sup>31,53</sup> Based on this we corrected the calculated CIS transition energies for  $(\text{HNO}_3)\cdot(\text{N}_2\text{O}_4)$ ,  $(\text{NO}_3^-)\cdot(\text{N}_2\text{O}_4)$  by 0.73 eV.

That is,

$$\Delta E_{(\text{corr})} = \Delta E_{(\text{CIS})} - 0.73 \text{ eV} \quad (6)$$

where  $\Delta E_{(\text{corr})}$  and  $\Delta E_{(\text{CIS})}$  are the corrected and uncorrected vertical excitation energies of the complexes, respectively.

The CIS results for isolated  $\text{N}_2\text{O}_4$  indicate that the transition between the ground and first excited state involves the promotion of an electron from a  $\sigma$ -bonding HOMO to a  $\pi$ -bonding LUMO, both located along the N–N axis of the molecule, in agreement with the DFT results Chesnut *et al.*<sup>81</sup> For  $(\text{HNO}_3)\cdot(\text{N}_2\text{O}_4)$  and  $(\text{NO}_3^-)\cdot(\text{N}_2\text{O}_4)$ , the CIS results indicate that the orbitals involved in the ground to first excited electronic state transition were very similar to those in isolated  $\text{N}_2\text{O}_4$ , supporting the application of

the energy correction described above. The corrected vertical excitation energy from the ground electronic state to the first excited electronic state of  $(\text{HNO}_3)\cdot(\text{N}_2\text{O}_4)$  is  $\Delta E_{(\text{corr})} = 3.69$  eV, or 336 nm. The intensity for the transition was nearly three times as strong as in isolated  $\text{N}_2\text{O}_4$  at  $f = 1.7 \times 10^{-4}$  [ $\sigma_{\text{A}}(336 \text{ nm}) = 1.8 \times 10^{-18} \text{ cm}^2$ , base 10]. The  $\Delta E_{(\text{corr})}$  for  $(\text{NO}_3^-)\cdot(\text{N}_2\text{O}_4)$  is 3.90 eV (318 nm), with an intensity of  $f = 9.3 \times 10^{-4}$  [ $\sigma_{\text{A}}(318 \text{ nm}) = 9.9 \times 10^{-18} \text{ cm}^2$ , base 10], more than an order of magnitude larger than in isolated  $\text{N}_2\text{O}_4$ . In both complexes, excitation involves the promotion of an electron from a  $\sigma$ -bonding orbital to the LUMO  $\pi$ -bonding orbital. In the case of  $(\text{NO}_3^-)\cdot(\text{N}_2\text{O}_4)$ , the  $\sigma$  orbital, which is not the HOMO, also has significant density on the  $\text{NO}_3^-$  subunit and therefore excitation to the  $\pi$ -orbital may destabilize the complex. These results indicate that  $(\text{HNO}_3)\cdot(\text{N}_2\text{O}_4)$  and  $(\text{NO}_3^-)\cdot(\text{N}_2\text{O}_4)$  are strong absorbers of light in the region above the 290 nm actinic cutoff,<sup>1</sup> indicating they may play an important role in initiating photochemistry that generates HONO or other volatile nitrogen species on surfaces.

### H-Atom transfer in $(\text{HNO}_3)\cdot(\text{N}_2\text{O}_4)$

A potential intramolecular hydrogen atom transfer reaction within the  $(\text{HNO}_3)\cdot(\text{N}_2\text{O}_4)$  complexes to form HONO was investigated by performing a series of constrained optimizations at multiple points along a plausible chemical reaction pathway using ROMP2/TZP, which was less problematic with regard to orbital convergence than B3LYP/TZP.

The postulated mechanism for H-atom transfer in  $(\text{HNO}_3)\cdot(\text{N}_2\text{O}_4)$  consisted of two steps and leads to the formation of a  $(\text{HONO})\cdot(\text{N}_2\text{O}_5)$  complex (Fig. 2). Step 1 consists of moving the H-atom of  $\text{HNO}_3$  incrementally from the  $\text{HNO}_3$  subunit



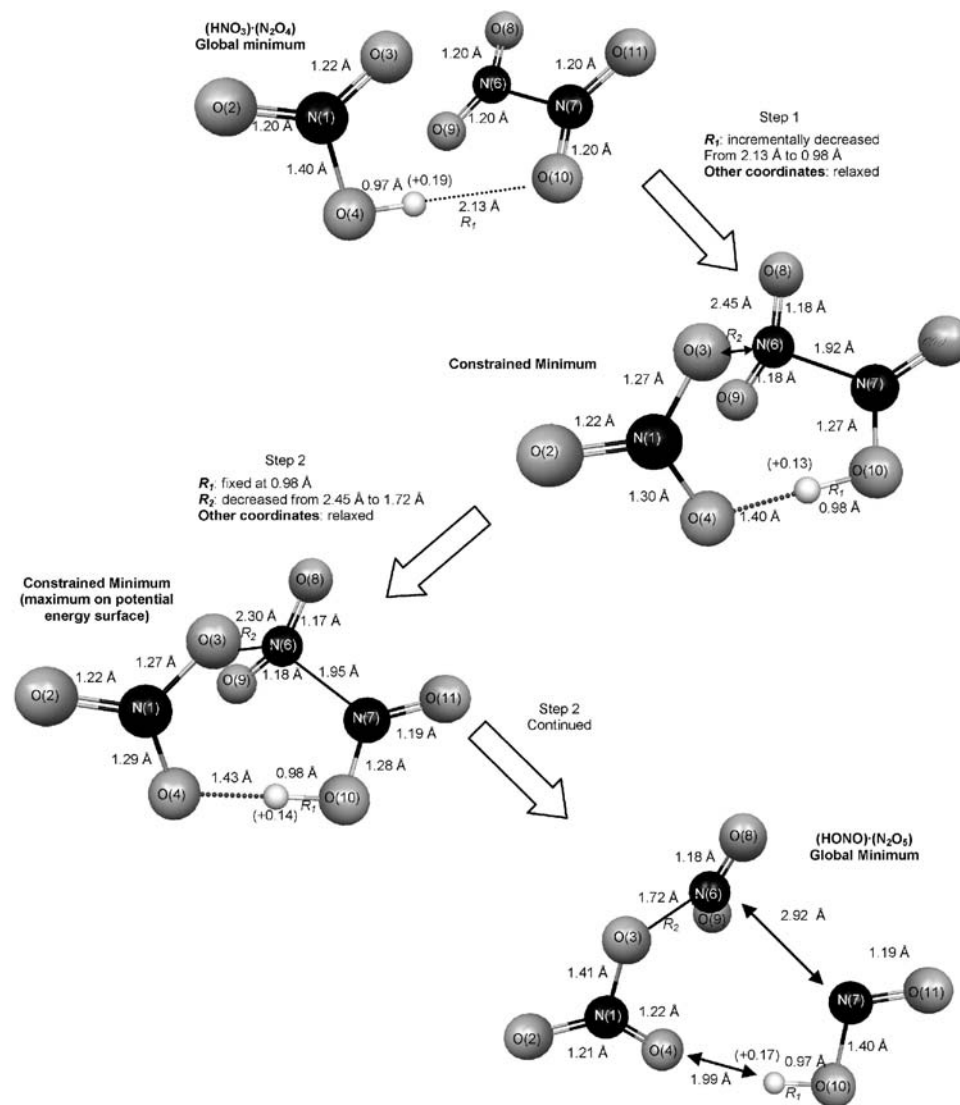


Fig. 2 Computed pathway for H-atom transfer within  $(\text{HNO}_3)\cdot(\text{N}_2\text{O}_4)$  to form  $(\text{HONO})\cdot(\text{N}_2\text{O}_5)$ .

toward O(10) of  $\text{N}_2\text{O}_4$  until a HONO moiety is formed. At this point the H–O distance in the HONO moiety is 0.98 Å, identical to the ROMP2/TZP value for isolated *trans*-HONO. A constrained optimization was then performed at each increment by fixing the O(10)··H distance  $R_1$  and allowing all other coordinates to optimize. The potential energy of each partially optimized structure is plotted as a function of  $R_1$  in Fig. 3a, and shows that the energy necessary to move the H-atom across the interior of the complex to  $\text{N}_2\text{O}_4$ , forming *trans*-HONO, is 41 kcal mol<sup>-1</sup>.

Step 2 proceeds by gradually decreasing the N(6)··O(3) distance  $R_2$  from 2.45 to 1.72 Å, forming an  $\text{N}_2\text{O}_5$ -like structure complexed to *trans*-HONO. A plot of the potential energy as a function of  $R_2$  (Fig. 3b) reveals a maximum of 34.5 kcal mol<sup>-1</sup> at  $R_2 = 2.3$  Å, with a structure corresponding to  $(\text{HONO})\cdot(\text{N}_2\text{O}_5)$ . As  $R_2$  increases the calculated bond order of the N(6)–N(7) bond decreases until it is less than 0.05 in the final structure of step 2. The H-atom charges for all structures depicted in Fig. 2 are between +0.19 and +0.17, suggesting

this reaction is truly a hydrogen atom transfer reaction and not a proton transfer reaction.

The energy barrier associated with the H-atom transfer within  $(\text{HNO}_3)\cdot(\text{N}_2\text{O}_4)$  to form  $(\text{HONO})\cdot(\text{N}_2\text{O}_5)$  was computed to be 40.9 kcal mol<sup>-1</sup>, corresponding to an excitation threshold of 702 nm. This estimate should be considered an upper limit for the true energy barrier of the reaction. The energy of the product complex was computed to be 17.4 kcal mol<sup>-1</sup> less than that of the maximum energy structure in Step 2, indicating the reaction is thermally irreversible; the barrier is too large to be overcome thermally or through a vibrational overtone excitation of the  $\text{HNO}_3$  O–H bond. However, a photochemical mechanism due to the absorption of solar radiation is possible. The  $(\text{HONO})\cdot(\text{N}_2\text{O}_5)$  formed has a moderate ROMP2 ZPE-corrected binding energy of –4.8 kcal mol<sup>-1</sup>, indicating that it is weakly stable and may dissociate to form volatile *trans*-HONO. It is likely that  $\text{H}_2\text{O}$  present on a surface will compete with  $\text{N}_2\text{O}_5$  for the HONO produced since the binding energy for the  $(\text{HONO})\cdot(\text{H}_2\text{O})$  complex is very similar at –5.3 kcal mol<sup>-1</sup>.<sup>23</sup> The  $\Delta E$  for the overall

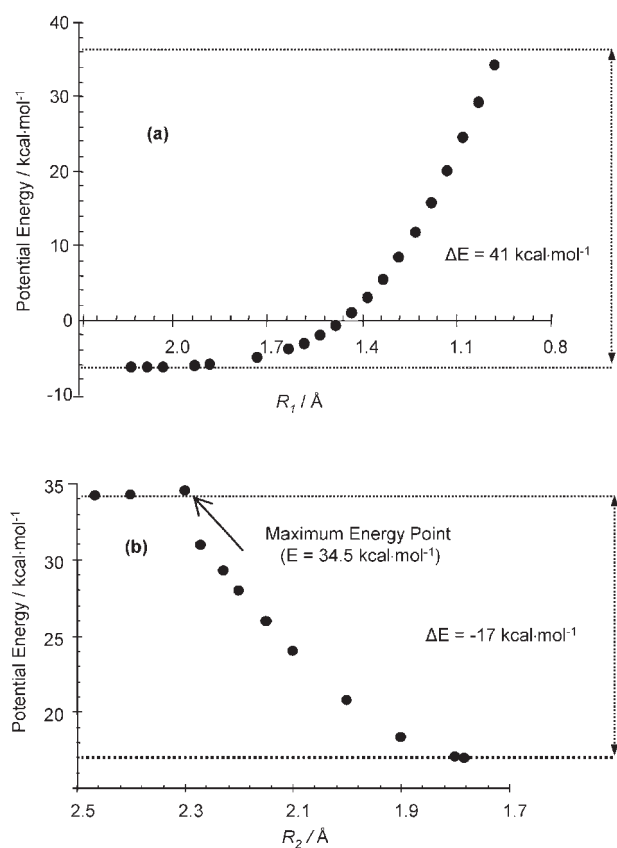


**Fig. 3** Energetics of the H-atom transfer mechanism in the  $(\text{HNO}_3)\cdot(\text{N}_2\text{O}_4)$  complex depicted in Fig. 2 showing potential energy *versus*: (a)  $R_1$  for step 1, and (b)  $R_2$  for step 2.

reaction  $\text{HNO}_3 + \text{N}_2\text{O}_4 \rightarrow \text{trans-HONO} + \text{N}_2\text{O}_5$  was computed to be  $22 \text{ kcal mol}^{-1}$ , in fair agreement with the experimental 298 K enthalpy  $\Delta H$  of  $14 \text{ kcal mol}^{-1}$  calculated using the NIST-JANAF Thermochemical Tables.<sup>82</sup>

### H-Atom transfer in $(\text{HNO}_3)\cdot(\text{NO}_2)$

H-Atom abstraction within the  $(\text{HNO}_3)\cdot(\text{NO}_2)$  complex was treated as a 3-step process (Fig. 4). In Step 1, the O(7) atom was rotated toward the  $\text{HNO}_3$  subunit by adjusting the torsion angle  $\tau$  defined by O(7), N(5), O(6), and O(3) from its equilibrium value of  $164^\circ$  to  $0^\circ$ . At  $\tau = 0^\circ$  O(7) points directly towards  $\text{HNO}_3$  and its partial negative charge is expected to reduce the energy required to transfer the H-atom. The potential energy values for the partially optimized structures (all internal coordinates optimized except for  $\tau$ ) are displayed as a function of  $\tau$  in Fig. 5a and show that the energy required to rotate O(7) towards  $\text{HNO}_3$  is only  $0.41 \text{ kcal mol}^{-1}$ .

In Step 2 the distance  $R_1$  between the H-atom of  $\text{HNO}_3$  and O(6) of the  $\text{NO}_2$  subunit was incrementally decreased from  $2.07 \text{ \AA}$  to the equilibrium O–H bond length of  $0.97 \text{ \AA}$  in the ROMP2/TZP optimized HONO. A plot of potential energy as a function of  $R_1$  (Fig. 5b) shows that transfer of the H-atom between the two subunits of the complex is accompanied by a rise in potential energy until a maximum is reached at  $49.7 \text{ kcal mol}^{-1}$ .

In Step 3, the  $\text{NO}_3$  subunit of the complex was gradually forced away from the H-atom. The internal coordinate  $R_2$ , which is the distance between the H-atom and the N of the

$\text{NO}_3$  subunit was incrementally adjusted from  $2.09$  to  $3.05 \text{ \AA}$  while  $R_2$  and  $R_1$  were fixed during the optimizations to prevent relaxation back to the reactants. The other internal coordinates were optimized. The potential energy of the system decreased with increasing  $R_2$  as shown in Fig. 5c. A full optimization was then performed on the  $R_2 = 3.05 \text{ \AA}$  structure to generate a local minimum for  $(\text{HONO})\cdot(\text{NO}_3)$  with an energy of  $46.2 \text{ kcal mol}^{-1}$ . Interestingly, the charge of the H-atom varies from  $+0.30$  in  $(\text{HNO}_3)\cdot(\text{NO}_2)$  to a high of  $+0.37$  in a transitional structure, and decreases to  $+0.23$  in  $(\text{HONO})\cdot(\text{NO}_3)$ ; Fig. 4. This indicates that the reaction can be thought of as part way between a proton transfer and H-atom transfer reaction.

Two other stable configurations of  $(\text{HONO})\cdot(\text{NO}_3)$  were located, having energies  $42.1 \text{ kcal mol}^{-1}$  and  $43.1 \text{ kcal mol}^{-1}$  greater than the combined energy of isolated  $\text{HNO}_3$  and  $\text{NO}_2$  (see the ESI†). All three  $(\text{HONO})\cdot(\text{NO}_3)$  complexes are weakly bound and should dissociate to produce surface HONO and  $\text{NO}_3$ . The HONO generated may immediately bind to  $\text{HNO}_3$ , the ROMP2/TZP ZPE-corrected binding energy of  $(\text{HONO})\cdot(\text{HNO}_3)$  is  $-3.5 \text{ kcal mol}^{-1}$ , only slightly stronger than  $(\text{HONO})\cdot(\text{NO}_3)$ . Therefore, we anticipate that surface water will displace HONO from the surface-bound  $(\text{HONO})\cdot(\text{HNO}_3)$  complex leading to volatilization of HONO. Alternatively, HONO may form a complex with  $\text{H}_2\text{O}$  on surfaces. The ZPE-corrected binding energy for the  $(\text{HONO})\cdot(\text{H}_2\text{O})$  complex was reported to be  $-5.3 \text{ kcal mol}^{-1}$ .<sup>23</sup>

The energy barrier for the H-atom abstraction/proton transfer within  $(\text{HNO}_3)\cdot(\text{NO}_2)$  to form  $(\text{HONO})\cdot(\text{NO}_3)$  is computed to be  $52.2 \text{ kcal mol}^{-1}$ . This corresponds to visible light with a wavelength of  $548 \text{ nm}$ . The potential energy of the product complex was computed to be just  $3.5 \text{ kcal mol}^{-1}$  lower than the potential energy of the maximum energy structure, indicating that the reaction is reversible. However, the  $\Delta E$  for the overall reaction  $\text{HNO}_3 + \text{NO}_2 \rightarrow \text{trans-HONO} + \text{NO}_3$  was computed to be  $46 \text{ kcal mol}^{-1}$ .

While this is significantly greater than the enthalpy of  $24 \text{ kcal mol}^{-1}$  calculated from the NIST-JANAF thermochemical tables,<sup>82</sup> it is still likely that HONO can be formed from H-atom transfer within the  $(\text{HNO}_3)\cdot(\text{NO}_2)$  complex *via* photoexcitation.

### ATR-FTIR investigation of $\text{HNO}_3\text{-NO}_x$ surface films

A series of ATR-FTIR experiments were carried out to search for complexes of  $\text{HNO}_3$  with  $\text{NO}_2$  or  $\text{N}_2\text{O}_4$  on the surface of a  $\text{SiO}_x$ -coated AMTIR internal reflection element (IRE). Initially the IRE was exposed to  $2.3 \text{ Torr}$  of anhydrous  $\text{HNO}_3$ . While this is a much larger concentration than found in the atmosphere, searching for the very existence of these complexes requires higher concentrations to obtain detectable signals. Fig. 6a shows bands due to surface-adsorbed  $\text{HNO}_3$  at  $1671$  and  $1303 \text{ cm}^{-1}$  assigned to the ONO-asymmetric stretch ( $\nu_{\text{as}}$ ) and mixed modes of the ONO-symmetric stretch ( $\nu_{\text{s}}$ ) and NOH bend ( $\delta$ ), respectively. The broad feature at  $1394 \text{ cm}^{-1}$  is the  $\nu_{3\text{a}}$  (antisymmetric  $\text{NO}_2$  stretch) of nitrate, present in small quantities on the surface.<sup>83</sup> Additional bands due to O–H stretches of  $\text{HNO}_3\cdot(\text{H}_2\text{O})_n$  ( $n = 1\text{--}3$ ) complexes were also observed in the present study between  $2400$  and  $3200 \text{ cm}^{-1}$  (not shown), similar to what was observed previously.<sup>22</sup> The presence of nitrate and nitric acid–water complexes

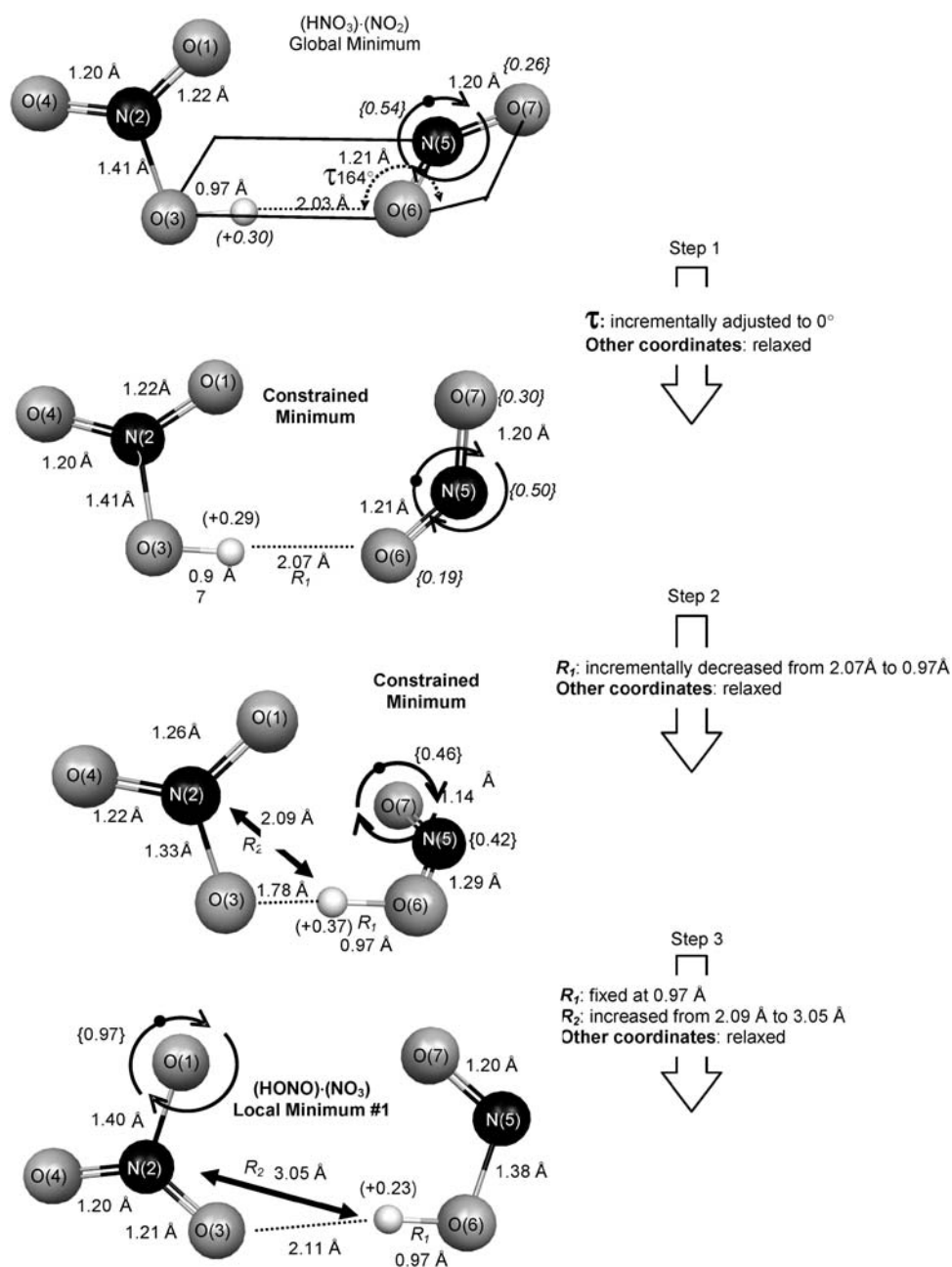


Fig. 4 Computed pathway for H-atom transfer within  $(\text{HNO}_3)\text{-(NO}_2)$  to form  $(\text{HONO})\text{-(NO}_3)$ .

suggests that residual water remains on the surface of the IRE, despite efforts to remove it under vacuum.

An infrared spectrum of species adsorbed to the surface of  $\text{SiO}_x$ -coated AMTIR during exposure to 2.3 Torr anhydrous  $\text{HNO}_3$  and 58 Torr of  $\text{NO}_2\text{-N}_2\text{O}_4$  is shown in Fig. 6b for the region  $800\text{--}1800\text{ cm}^{-1}$ . The spectrum was obtained by taking the ratio of the single beam spectrum in the presence of a mixture of  $\text{HNO}_3\text{-NO}_2\text{-N}_2\text{O}_4$  to that of anhydrous  $\text{HNO}_3$  shown in Fig. 6a. Absorption bands attributed to  $\text{HNO}_3$  are present at  $1667$  and  $1303\text{ cm}^{-1}$ . Strong bands at  $1743$  and  $1256\text{ cm}^{-1}$  are related to surface-adsorbed  $\text{N}_2\text{O}_4$ , as confirmed by comparison to a reference spectrum obtained by exposing a clean  $\text{SiO}_x$ -AMTIR surface to 84 Torr of  $\text{NO}_2\text{-N}_2\text{O}_4$  (Fig. 6c).

As discussed below, these are assigned to  $\text{N}_2\text{O}_4$  complexed to  $\text{HNO}_3$  and  $\text{NO}_3^-$ . The reference spectrum of  $\text{NO}_2\text{-N}_2\text{O}_4$  has weak features in the region  $1300\text{--}1700\text{ cm}^{-1}$  that coincide with peaks shown in Fig. 6b. These arise from the reaction of  $\text{N}_2\text{O}_4$  with residual water on the  $\text{SiO}_x$ -coated AMTIR surface to form nitric acid complexes.

New bands at  $1632$  and  $1602\text{ cm}^{-1}$  appear in the spectrum obtained when the IRE is exposed to an  $\text{HNO}_3\text{-NO}_2\text{-N}_2\text{O}_4$  mixture. These peaks disappeared when the reaction chamber was evacuated, suggesting that species responsible for these peaks are not held on the surface by strong interactions. The band at  $1632\text{ cm}^{-1}$  in Fig. 6b is attributed to the  $\nu_{\text{as}}(\text{NO}_2)$  of  $\text{NO}_2$  complexed to  $\text{NO}_3^-$ , in agreement with the *ab initio*

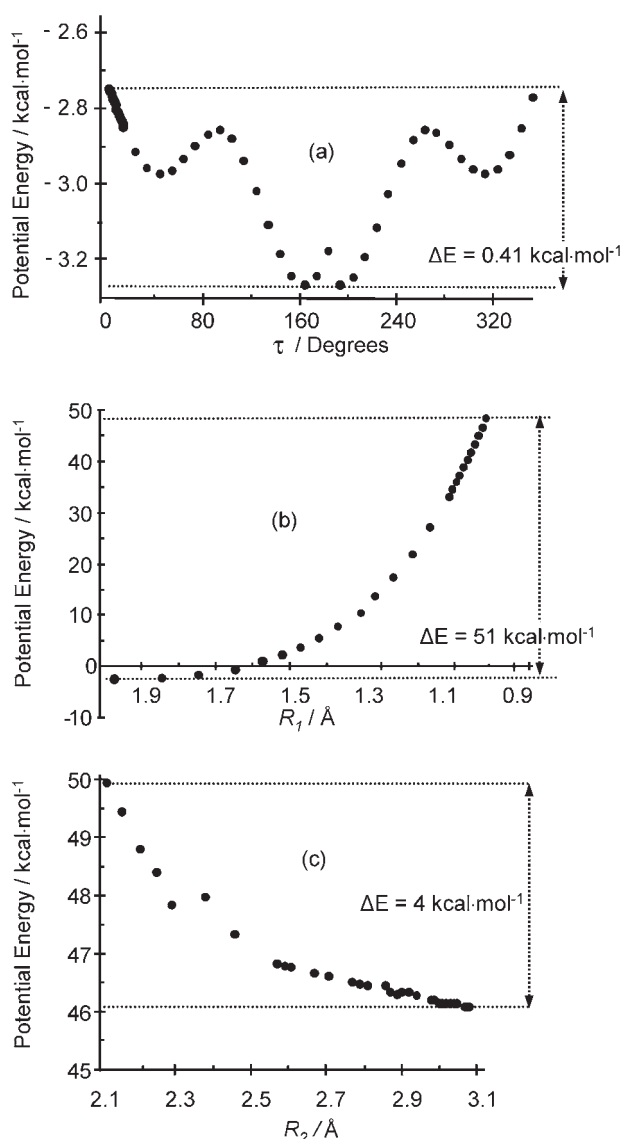


**Fig. 5** Energetics of the H-atom transfer in the  $(\text{HNO}_3)\cdot(\text{NO}_2)$  complex depicted in Fig. 4 showing potential energy *versus*: (a)  $\tau$  for step 1, (b)  $R_1$  for step 2, and (c)  $R_2$  for step 3.

calculations that predict a  $+11\text{ cm}^{-1}$  shift in this mode relative to free  $\text{NO}_2$  (Table 4). The band at  $1602\text{ cm}^{-1}$  is assigned to the  $\nu_{\text{as}}(\text{NO}_2)$  of nitrogen dioxide in the  $(\text{HNO}_3)\cdot(\text{NO}_2)$  complex. This is based on the ROMP2/TZP infrared frequencies that predict an insignificant shift for the  $\nu_{\text{as}}(\text{NO}_2)$  mode of  $(\text{HNO}_3)\cdot(\text{NO}_2)$  relative to free  $\text{NO}_2$ , and the lack of detectable amounts of  $\text{NO}_2$  on surfaces in the absence of  $\text{HNO}_3$ . In recent experiments using ATR-FTIR to study the hydrolysis of  $\text{NO}_2$  on surfaces, Ramazan *et al.*<sup>22</sup> observed a peak at  $1600\text{ cm}^{-1}$  under conditions closer to those found in a polluted atmosphere. In their study of  $(\text{HNO}_3)\cdot(\text{NO}_2)$  in a frozen argon matrix, Barnes *et al.*<sup>32</sup> reported a band centered at  $1606\text{ cm}^{-1}$ , shifted by just  $-5\text{ cm}^{-1}$  with respect to the  $\nu_{\text{as}}$  band of  $\text{NO}_2$  observed in the absence of  $\text{HNO}_3$ . Barnes *et al.*<sup>32</sup> also reported bands at  $3441$  and  $561\text{ cm}^{-1}$  and attributed them to the O–H stretch and NOH torsion of the  $(\text{HNO}_3)\cdot(\text{NO}_2)$  complex. A band at  $3441\text{ cm}^{-1}$  was absent from our spectra of the  $\text{HNO}_3\text{--NO}_2\text{--N}_2\text{O}_4$  mixture,

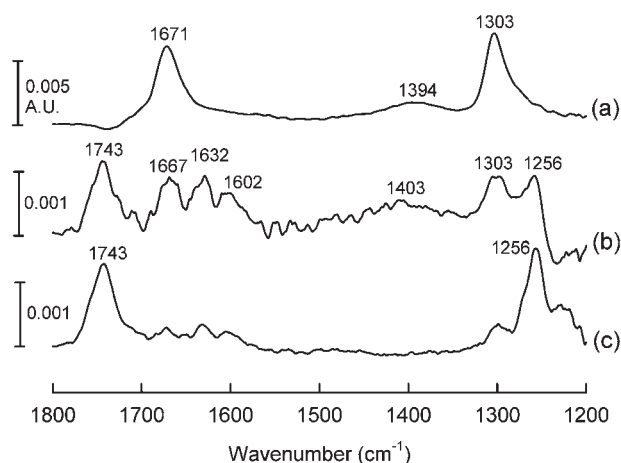


**Fig. 6** Spectrum of  $\text{SiO}_x$ -coated AMTIR crystal exposed to (a) 2.3 Torr anhydrous  $\text{HNO}_3$  only; (b) 2.3 Torr anhydrous  $\text{HNO}_3$  and 46 Torr of  $\text{NO}_2\text{--N}_2\text{O}_4$ ; (c) 84 Torr of  $\text{NO}_2\text{--N}_2\text{O}_4$  only.

but this is not surprising since this is expected to be very broad under the conditions of the experiment. The NOH torsion lies outside the spectral range of the IRE and detector used.

We assign the bands at  $1743$  and  $1256\text{ cm}^{-1}$  to  $\nu_{\text{s}}(\text{NO}_2)$  and  $\nu_{\text{as}}(\text{NO}_2)$  of  $\text{N}_2\text{O}_4$  complexed to  $\text{HNO}_3$  and  $\text{NO}_3^-$ . The peaks in Fig. 6b are indistinguishable from  $\text{N}_2\text{O}_4$  on the surface in the absence of added  $\text{HNO}_3$  or  $\text{NO}_3^-$ . However, calculations predict shifts of  $+15\text{ cm}^{-1}$  at the most for  $\nu_{\text{as}}(\text{NO}_2)$  stretches of  $\text{N}_2\text{O}_4$  upon complexation with  $\text{HNO}_3$  and such differences will not be easily distinguishable due to the broad peaks in these experiments. The fact that  $\text{N}_2\text{O}_4$  is observed on the surface in Fig. 6b and c and that enhanced levels of  $\text{N}_2\text{O}_4$  have been observed on surfaces containing nitric acid in other systems<sup>20,21,27</sup> suggests that  $\text{N}_2\text{O}_4$  forms complexes with  $\text{HNO}_3$  or  $\text{NO}_3^-$  on surfaces.

This is supported by calculated equilibrium constants for  $(\text{HNO}_3)\cdot(\text{NO}_2)$  and  $(\text{HNO}_3)\cdot(\text{N}_2\text{O}_4)$ , which are  $0.007\text{ atm}^{-1}$  and  $0.25\text{ atm}^{-1}$  at  $298\text{ K}$ , respectively. Under the present conditions, this would correspond to a concentration of  $(\text{HNO}_3)\cdot(\text{N}_2\text{O}_4)$  that is  $\sim 15$  times higher than  $(\text{HNO}_3)\cdot(\text{NO}_2)$ . Although all calculations here are for the gas-phase rather than for complexes on surfaces, the trend is consistent with the observations shown in Fig. 6c where the area of the peak at  $1743\text{ cm}^{-1}$  is approximately double that of the peak at  $1602\text{ cm}^{-1}$ . As seen in Fig. 6c, even trace amounts of water will lead to  $\text{HNO}_3$  formation in the presence of  $\text{N}_2\text{O}_4$  and subsequent formation of nitric acid–nitrate complexes will lead to enhanced uptake of  $\text{N}_2\text{O}_4$  on the surface. We also considered the possibility that  $\text{N}_2\text{O}_4$  is complexed to  $\text{SiOH}$  on the IRE surface.<sup>84</sup> Complexes of  $\text{HNO}_3$  and  $\text{N}_2\text{O}_4$  with free OH groups on the IRE surface are formed during initial exposure to  $\text{N}_2\text{O}_4$ , as indicated by a reduction of free  $\text{SiOH}$  stretch at  $3650\text{--}3800\text{ cm}^{-1}$ . However, the surface quickly saturates and the  $\nu(\text{SiO--H})$  peak intensity remains constant, while peaks attributed to  $\text{N}_2\text{O}_4$  continue to increase in intensity linearly with  $\text{NO}_2/\text{N}_2\text{O}_4$  concentration due to further complexation to  $\text{HNO}_3$  and  $\text{NO}_3^-$ .

### UV/visible spectrum of $\text{N}_2\text{O}_4$ in aqueous nitric acid

Fig. 7 shows the UV/vis absorption spectra of  $\text{N}_2\text{O}_4$  dissolved in concentrated  $\text{HNO}_3$  and in acetonitrile, respectively. For

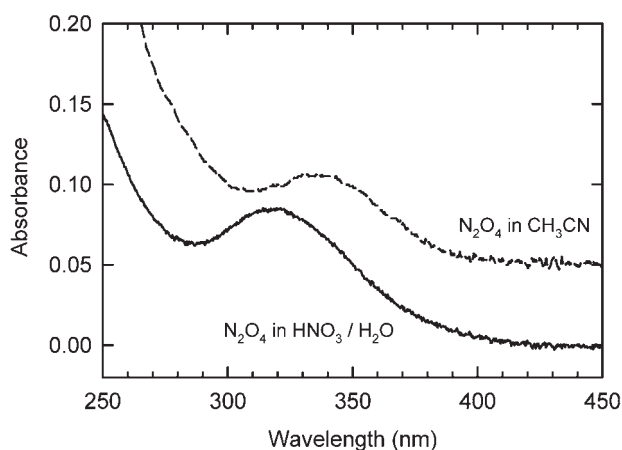


**Fig. 7** UV/vis absorption spectra of (a)  $\text{N}_2\text{O}_4$  dissolved in a solution of 70% w/w  $\text{HNO}_3$ - $\text{H}_2\text{O}$  (solid line) and (b)  $\text{N}_2\text{O}_4$  dissolved in anhydrous acetonitrile (spectrum shifted along y-axis for clarity). The spectrum in  $\text{N}_2\text{O}_4$  in  $\text{HNO}_3$  was obtained by subtracting from the spectrum of a solution of  $\text{HNO}_3$ - $\text{H}_2\text{O}$  from a spectrum of  $\text{HNO}_3$ - $\text{H}_2\text{O}$ - $\text{N}_2\text{O}_4$ .

solutions of  $\text{N}_2\text{O}_4$  in  $\text{HNO}_3$ - $\text{H}_2\text{O}$ , a distinct band is observed centered at 320 nm with a tail that extends out to 340 nm. In the  $\text{N}_2\text{O}_4$ -acetonitrile spectrum, there is an absorbance band centered at 338 nm, similar to what is observed for  $\text{N}_2\text{O}_4$  dissolved in hexane ( $\lambda_{\text{max}} = 343 \text{ nm}$ )<sup>85</sup> and methylene chloride ( $\lambda_{\text{max}} \approx 340 \text{ nm}$ ).<sup>86</sup> The band center locations in the UV/vis spectra of  $\text{N}_2\text{O}_4$  in acetonitrile, hexane, and methylene chloride are very similar to the band center location in the spectrum of gaseous  $\text{N}_2\text{O}_4$ .<sup>30</sup> This is expected since there is a lack of strong solute-solvent interactions in these mixtures. The approximately 20 nm blue shift in the absorbance band of  $\text{N}_2\text{O}_4$  in concentrated nitric acid relative to  $\text{N}_2\text{O}_4$  in organic solvents having minimal solvent-solute interactions is in excellent agreement with the -22 nm shift in the vertical excitation energies of  $(\text{NO}_3^-)(\text{N}_2\text{O}_4)$  relative to isolated  $\text{N}_2\text{O}_4$  derived from CIS calculations. It was not possible to determine the molar absorption coefficients for the  $\text{HNO}_3$ - $\text{N}_2\text{O}_4$  solution since the path-length between the quartz coverslips used to contain the solutions was indeterminate. Solutions in cuvettes with longer and defined pathlengths absorbed too strongly at wavelengths less than 340 nm to resolve the  $\text{N}_2\text{O}_4$  absorption band.

Formation of the  $(\text{NO}_3^-)(\text{N}_2\text{O}_4)$  complex in concentrated  $\text{HNO}_3$  requires the presence of  $\text{NO}_3^-$ . While undissociated  $\text{HNO}_3$  is favored in concentrated solutions of  $\text{HNO}_3$ , spectroscopic studies have shown  $\text{NO}_3^-$  is present in such solutions, due in part to the ionization of  $\text{N}_2\text{O}_4$ .<sup>87,88</sup> The UV/vis absorption spectra presented here support the existence of the  $(\text{NO}_3^-)(\text{N}_2\text{O}_4)$  complex and is consistent with the enhancement of visible light absorption for solutions of  $\text{N}_2\text{O}_4$  and  $\text{HNO}_3$ .

## Atmospheric implications

$\text{HNO}_3$  and  $\text{NO}_3^-$  are ubiquitous components of urban surface films,<sup>89</sup> resulting from heterogeneous chemistry such as  $\text{NO}_2$  and  $\text{N}_2\text{O}_5$  hydrolysis, and deposition of  $\text{HNO}_3$  and nitrate-containing particles.<sup>1</sup>  $\text{HNO}_3$  and  $\text{NO}_3^-$  are considered “end

products” of atmospheric oxidation of gaseous nitrogen oxides emitted during fossil fuel combustion. Consequently,  $\text{NO}_x$  will be present near boundary layer surfaces that hold the acid and the anion, creating conditions favorable for forming the type of complexes investigated here.

The calculations show that complexes of  $\text{N}_2\text{O}_4$  with  $\text{HNO}_3$  and  $\text{NO}_3^-$  are more stable than those with  $\text{NO}_2$ , and hence more likely to play a role in heterogeneous chemistry at room temperature. One argument against a significant role for  $\text{N}_2\text{O}_4$  is that the concentrations in equilibrium with atmospherically relevant concentrations of  $\text{NO}_2$  are quite small, since the equilibrium constant<sup>90</sup> for the  $2\text{NO}_2 \leftrightarrow \text{N}_2\text{O}_4$  reaction is only  $2.8 \times 10^{-19} \text{ cm}^3 \text{ molecule}^{-1}$ . For example, at 100 ppb  $\text{NO}_2$ , the concentration of  $\text{N}_2\text{O}_4$  in equilibrium with it is only 0.07 ppt in the gas phase. However, the gas-phase equilibrium does not accurately represent condensed phase  $\text{N}_2\text{O}_4$  concentrations. Experimental evidence<sup>87,91</sup> suggests that  $\text{N}_2\text{O}_4$  is the dominant species formed in solution, with solution phase equilibrium constants 3–4 orders of magnitude higher than the gas-phase equilibrium.<sup>92</sup> The stability of the  $\text{N}_2\text{O}_4$  complexes with  $\text{HNO}_3$  and  $\text{NO}_3^-$  predicted here suggests that the surface concentration of  $\text{N}_2\text{O}_4$  may also be larger than expected from the gas phase equilibrium.<sup>21</sup> The amount of the surface-bound dimer may be limited by the amount of available adsorbed  $\text{HNO}_3$  and  $\text{NO}_3^-$ . Therefore, one may expect surfaces to hold increasing amounts of  $\text{N}_2\text{O}_4$  in the form of the complexes as more complexing species are generated in such reactions as (1) and the hydrolysis of  $\text{N}_2\text{O}_5$ .

Some of these complexes may play a key role in the thermal reaction (1). For example, the source of the surface  $\text{N}_2\text{O}_4$  could be a sequential complexation of  $\text{NO}_2$  to  $\text{HNO}_3$  to form  $(\text{HNO}_3)(\text{NO}_2)$  and then  $(\text{HNO}_3)(\text{O}_2\text{NNO}_2)$  or  $(\text{HNO}_3)(\text{ONONO}_2)$ . In any event, if there is an equilibrium concentration of  $(\text{HNO}_3)(\text{NO}_2)$  complexes on the surface and the rate determining step for forming  $(\text{HNO}_3)(\text{ONONO}_2)$  and then  $\text{HONO} + \text{HNO}_3$  is uptake of  $\text{NO}_2$  from the gas phase, the formation of  $\text{HONO}$  would be first order in gas phase  $\text{NO}_2$ , consistent with experimental observations.<sup>5,27,93–100</sup> It is also possible that the  $(\text{HNO}_3)(\text{N}_2\text{O}_4)$  will be only short-lived and spontaneously undergo ionization to  $\text{NO}^+\text{NO}_3^-$ , followed by protonation to yield  $\text{HONO}$  and  $\text{HNO}_3$ . The present studies also show that the photochemically driven transfer of a hydrogen atom from  $\text{HNO}_3$  to  $\text{NO}_2$  and  $\text{N}_2\text{O}_4$  to form  $\text{HONO}$  are feasible.

The calculations presented here show that  $\text{N}_2\text{O}_4$  does indeed lend its photochemical properties to the complexes with  $\text{HNO}_3$  and  $\text{NO}_3^-$ . The peak of the transition to the first excited state for  $\text{N}_2\text{O}_4$  alone is centered at 340 nm, but the absorption band is broad and extends beyond 430 nm.<sup>101</sup> This suggests that light absorption by the  $(\text{HNO}_3)(\text{N}_2\text{O}_4)$  and  $(\text{NO}_3^-)(\text{N}_2\text{O}_4)$  complexes, which are predicted to occur at 336 and 318 nm, respectively, will also extend out into the visible region. The N–N bond energy of  $\text{N}_2\text{O}_4$  is  $12.7 \text{ kcal mol}^{-1}$ ,<sup>102</sup> much less than the excitation energy of the chromophore. Therefore, the adsorption of a photon by the  $(\text{HNO}_3)(\text{N}_2\text{O}_4)$  complex may result in fragmentation of  $\text{N}_2\text{O}_4$  into electronically excited  $\text{NO}_2^*$  and a ground state  $\text{NO}_2$ , similar to what is observed in the photodissociation of free  $\text{N}_2\text{O}_4$ .<sup>103</sup> The electronically excited  $\text{NO}_2^*$  generated during this process may react with water or  $\text{HNO}_3$  on the surface, analogous to what was proposed by Li *et al.* in the gas phase.<sup>33</sup>

It is intriguing that irradiation of humidified air in the SAPHIR chamber produced HONO at a rate of 0.391 ppb h<sup>-1</sup> with the 370 nm cutoff filter in place and 0.665 ppb h<sup>-1</sup> for the experiment without the filter.<sup>26</sup> This is only a factor of 1.7 decrease in the HONO production rate, and should be much larger if HNO<sub>3</sub>, NO<sub>3</sub><sup>-</sup>, or N<sub>2</sub>O<sub>4</sub> were the precursors. This and the fact that HONO production could be parameterized based on NO<sub>2</sub> photolysis is consistent with surface (HNO<sub>3</sub>)·(NO<sub>2</sub>) or (NO<sub>3</sub><sup>-</sup>)·(NO<sub>2</sub>) being the photolytic HONO precursor. In the case of (NO<sub>3</sub><sup>-</sup>)·(NO<sub>2</sub>), electronically excited NO<sub>2</sub> would abstract a proton from water or nitric acid co-adsorbed on the surface. While the photochemical evidence favors this explanation, the weak gas-phase binding energy of especially (HNO<sub>3</sub>)·(NO<sub>2</sub>) would seem to preclude it from being the HONO source in the SAPHIR experiments. Conversely, the complexes (HNO<sub>3</sub>)·(N<sub>2</sub>O<sub>4</sub>) and (NO<sub>3</sub><sup>-</sup>)·(N<sub>2</sub>O<sub>4</sub>) that have substantial binding energies to hold NO<sub>x</sub> to surfaces, absorb light at λ < 370 nm and do not explain the HONO production rates in the cutoff filter experiments. However, it should be emphasized that the binding energies calculated here are for gas-phase species and the interactions between NO<sub>2</sub> and HNO<sub>3</sub> and NO<sub>3</sub> may be very different in surface films comprised of complex mixtures.

The present calculations did not include water which is present on all surfaces in the lower atmosphere. Infrared spectroscopic studies show that at 50% relative humidity during the NO<sub>2</sub> heterogeneous hydrolysis, the major hydrate of HNO<sub>3</sub> on the surface is the monohydrate.<sup>22</sup> The binding energy of HNO<sub>3</sub> to one water molecule in the gas phase is calculated to be ~8 kcal mol<sup>-1</sup>,<sup>23,104,105</sup> similar to the binding energy of 7 kcal mol<sup>-1</sup> for HNO<sub>3</sub> to N<sub>2</sub>O<sub>4</sub> calculated here (Table 1). The role of water is more complex than simply binding to surface species, however, since it also assists in the isomerization<sup>106</sup> of symmetric to asymmetric N<sub>2</sub>O<sub>4</sub> and reacts with the autoionized NO<sup>+</sup>NO<sub>3</sub><sup>-</sup> to form HONO and HNO<sub>3</sub> on the surface.

Furthermore, water has been shown to displace HONO from surfaces into the gas phase in both laboratory and field studies.<sup>107,108</sup> Whether this is a simple competitive adsorption/desorption process or a chemical reaction with a HONO precursor is not known. However, if a complex such as (HNO<sub>3</sub>)·(N<sub>2</sub>O<sub>4</sub>) is a precursor to HONO, the latter may be initially bound to HNO<sub>3</sub> when it is formed on the surface. The release of HONO upon the addition of water vapor or increase in the relative humidity may be due to stronger binding of H<sub>2</sub>O to HNO<sub>3</sub> than of HONO to HNO<sub>3</sub>, thus causing HONO to be displaced. We have computed the ROMP2 binding energy of the (HNO<sub>3</sub>)·(HONO) complex. The ZPE corrected binding energy of this complex is -3.5 kcal mol<sup>-1</sup> and is small compared with the binding energy for (HNO<sub>3</sub>)·(H<sub>2</sub>O) complex, which is about -7 to -10 kcal mol<sup>-1</sup>.<sup>59,60</sup>

In summary, the calculations presented here highlight the potential importance of HNO<sub>3</sub> and NO<sub>3</sub><sup>-</sup> complexes with oxides of nitrogen on surfaces. Such complexes may be key intermediates in the thermal and photochemical production of HONO in the absence of organic compounds.

## Acknowledgements

We are grateful to the National Science Foundation for support of this work through the Environmental Molecular

Sciences Institute (grant number 0431512). We thank Prof. Mark Bachmann and his group at the UCI Integrated Nanosystems Research Facility for providing plasma-enhanced chemical vapor deposition capabilities. L.F.P. thanks the Erskine Fund of the University of Canterbury for assistance with travel expenses. We also thank Dr Sotiris Xantheas at Pacific Northwest National Laboratory for helpful discussions and comments on the manuscript.

## References

- B. J. Finlayson-Pitts and J. N. Pitts, Jr, *Chemistry of the Upper and Lower Atmosphere—Theory, Experiments, and Applications*, Academic Press, San Diego, 2000.
- A. M. Winer and H. W. Biermann, *Res. Chem. Intermed.*, 1994, **20**, 403–445.
- B. Alicke, U. Platt and J. Stutz, *J. Geophys. Res.*, [Atmos.], 2002, **107**, , DOI: 10.1029/2000JD000075.
- J. Stutz, B. Alicke and A. Neftel, *J. Geophys. Res.*, [Atmos.], 2002, **107**, , DOI: 10.1029/2001JD000390.
- J. Kleffmann, K. H. Becker and P. Wiesen, *Atmos. Environ.*, 1998, **32**, 2721–2729.
- J. Kleffmann, T. Gavriloaiei, A. Hofzumahaus, F. Holland, R. Koppmann, L. Rupp, E. Schlosser, M. Siese and A. Wahner, *Geophys. Res. Lett.*, 2005, **32**, L05818.
- X. Zhou, H. J. Beine, R. E. Honrath, J. D. Fuentes, W. Simpson, P. B. Shepson and J. W. Bottenheim, *Geophys. Res. Lett.*, 2001, **28**, 4087–4090.
- X. Zhou, K. Civerolo, H. Dai, G. Huang, J. Schwab and K. Demerjian, *J. Geophys. Res.*, [Atmos.], 2002, **107**.
- H. Akimoto, H. Takagi and F. Sakamaki, *Int. J. Chem. Kinet.*, 1987, **19**, 539–551.
- X. Zhou, H. Gao, Y. He, G. Huang, S. B. Bertman, K. Civerolo and J. Schwab, *Geophys. Res. Lett.*, 2003, **30**, , DOI: 10.1029/2003GL018620.
- K. A. Ramazan, D. Syomin and B. J. Finlayson-Pitts, *Phys. Chem. Chem. Phys.*, 2004, **6**, 3836–3843.
- C. George, R. S. Strekowski, J. Kleffmann, K. Stemmler and M. Ammann, *Faraday Discuss.*, 2005, **130**, 195–210.
- I. Bejan, Y. Abd El Aal, I. Barnes, T. Benter, B. Bohn, P. Wiesen and J. Kleffmann, *Phys. Chem. Chem. Phys.*, 2006, **8**, 2028–2035.
- K. Stemmler, M. Ammann, C. Donders, J. Kleffmann and C. George, *Nature*, 2006, **440**, 195–198.
- X. Zhou, Y. Hi, G. Huang, T. D. Thornberry, M. A. Carroll and S. B. Bertman, *Geophys. Res. Lett.*, 2002, **29**, , DOI: 10.1029/2002GL015080.
- F. Rohrer, B. Bohn, T. Brauers, D. Bruning, F. J. Johnen, A. Wahner and J. Kleffmann, *Atmos. Chem. Phys.*, 2005, **5**, 2189–2201.
- W. P. L. Carter, R. Atkinson, A. M. Winer and J. N. J. Pitts, *Int. J. Chem. Kinet.*, 1981, **13**, 735–740.
- W. P. L. Carter, R. Atkinson, A. M. Winer and J. N. J. Pitts, *Int. J. Chem. Kinet.*, 1982, **14**, 1071–1103.
- W. P. L. Carter, R. Atkinson, A. M. Winer and J. N. Pitts, *Atmos. Environ.*, 1985, **19**, 1977–1978.
- A. L. Goodman, G. M. Underwood and V. H. Grassian, *J. Phys. Chem. A*, 1999, **103**, 7217–7223.
- W. S. Barney and B. J. Finlayson-Pitts, *J. Phys. Chem. A*, 2000, **104**, 171–175.
- K. A. Ramazan, L. M. Wingen, Y. Miller, G. M. Chaban, R. B. Gerber, S. S. Xantheas and B. J. Finlayson-Pitts, *J. Phys. Chem. A*, 2006, **110**, 6886–6897.
- M. Staikova and D. J. Donaldson, *Phys. Chem. Chem. Phys.*, 2001, **3**, 1999–2006.
- J. Mack and J. R. Bolton, *J. Photochem. Photobiol., A*, 1999, **128**, 1–13.
- H. Herrmann, *Phys. Chem. Chem. Phys.*, 2007, **9**, 3935–3964.
- F. Rohrer, B. Bohn, T. Brauers, D. Bruning, F. J. Johnen, A. Wahner and J. Kleffmann, *Atmos. Chem. Phys.*, 2005, **5**, 2189–2201.
- B. J. Finlayson-Pitts, L. M. Wingen, A. L. Sumner, D. Syomin and K. A. Ramazan, *Phys. Chem. Chem. Phys.*, 2003, **5**, 223–242.
- A. S. Pimentel, F. C. A. Lima and A. B. F. da Silva, *J. Phys. Chem. A*, 2007, **111**, 2913–2920.

- 29 A. S. Pimentel, F. C. A. Lima and A. B. F. da Silva, *Chem. Phys. Lett.*, 2007, **436**, 47–50.
- 30 M. H. Harwood and R. L. Jones, *J. Geophys. Res., [Atmos.]*, 1994, **99**, 22955–22964.
- 31 T. C. Hall and F. E. Blacet, *J. Chem. Phys.*, 1952, **20**, 1745–1749.
- 32 A. J. Barnes, E. Lasson and C. J. Nielsen, *J. Mol. Struct.*, 1994, **322**, 165–174.
- 33 S. Li, J. Matthews and A. Sinha, *Science*, 2008, **21**, 1657–1660.
- 34 J. N. Crowley and S. A. Carl, 23, 1997, **101**, 4178–4184.
- 35 P. O. Wennberg and D. Dabdub, *Science*, 2008, **319**, 1624–1625.
- 36 T. Berces and S. Forgeteg, *Trans. Faraday Soc.*, 1970, **66**, 640–647.
- 37 S. Jaffe and H. W. Ford, *J. Phys. Chem.*, 1967, **71**, 1832–1835.
- 38 H. S. Johnston, S. G. Chang and G. Whitten, *J. Phys. Chem.*, 1974, **78**, 1–7.
- 39 C. C. J. Roothaan, *Rev. Mod. Phys.*, 1960, **32**, 179–185.
- 40 C. Lee, W. Yang and R. G. Parr, *Phys. Rev. B*, 1988, **37**, 785–789.
- 41 A. D. Becke, *Phys. Rev. A*, 1988, **38**, 3098–3110.
- 42 A. D. Becke, *J. Chem. Phys.*, 1992, **96**, 2155–2160.
- 43 C. Moeller and M. S. Plesset, *Phys. Rev.*, 1934, **46**, 618–622.
- 44 T. H. Dunning, *J. Chem. Phys.*, 1971, **55**, 716–723.
- 45 Y. Miller, G. M. Chaban and R. B. Gerber, *Chem. Phys.*, 2005, **313**, 213–224.
- 46 P. O. Lowdin, *Adv. Quantum Chem.*, 1970, **5**, 185–189.
- 47 R. C. Hilborn, *Am. J. Phys.*, 1982, **50**, 982–986.
- 48 J. B. Foresman, M. Head-Gordon, J. A. Pople and M. J. Frish, *J. Phys. Chem.*, 1992, **96**, 135–149.
- 49 P. G. Jasien and L. L. Weber, *THEOCHEM*, 2001, **572**, 203–212.
- 50 J. Abe and Y. Shirai, *J. Am. Chem. Soc.*, 1996, **118**, 4705–4706.
- 51 D. T. Major and B. Fischer, *J. Phys. Chem. A*, 2003, **107**, 8923–8931.
- 52 W. Bartkowiak and P. Lipkowski, *J. Mol. Model.*, 2005, **11**, 317–322.
- 53 A. M. Bass, A. E. L., Jr and A. H. Laufer, *J. Res. Natl. Bur. Stand. Sect. A*, 1976, **80**, 143–166.
- 54 M. S. Gordon and M. W. Schmidt, in *Theory and Applications of Computational Chemistry: the First Forty Years*, ed. C. E. Dykstra, G. Frenking, K. S. Kim and G. E. Scuseria, Elsevier, Amsterdam, 2005, pp. 1167–1189.
- 55 M. W. Schmidt, K. K. Baldrige, J. A. Boatz, S. T. Elbert, M. S. Gordon, J. H. Jensen, S. Koseki, N. Matsunaga, K. A. Nguyen, S. Su, T. L. Windus, M. Dupuis and J. A. Montgomery, *J. Comput. Chem.*, 1993, **14**, 1347–1363.
- 56 A. Komornicki and J. W. McIver, *J. Chem. Phys.*, 1979, **70**, 2014–2016.
- 57 Z. Rahim and B. N. Barman, *Acta Crystallogr., Sect. A*, 1978, **34**, 761–764.
- 58 S. Scheiner, *Annu. Rev. Phys. Chem.*, 1994, **45**, 23–56.
- 59 J. R. Scott and J. B. Wright, *J. Phys. Chem. A*, 2004, **108**, 10578–10585.
- 60 F.-M. Tao, K. Higgins, W. Klemperer and D. D. Nelson, *Geophys. Res. Lett.*, 1996, **23**, 1797–1800.
- 61 Y. Dimitrova and S. Peyerimhoff, *Chem. Phys.*, 2000, **254**, 125–134.
- 62 D. Goebel, U. Hohm, K. Kerl, U. Trumper and G. Maroulis, *J. Phys. Chem.*, 1994, **98**, 13123–13130.
- 63 W. A. Guillory and M. L. Bernstein, *J. Chem. Phys.*, 1975, **62**, 1058–1060.
- 64 P. R. McCurdy, W. P. Hess and S. S. Xantheas, *J. Phys. Chem. A*, 2002, **106**, 7628–7635.
- 65 Y. Elyoussofi, M. Herman, J. Lievin and I. Kleiner, *Spectrochim. Acta, Part A*, 1997, **53**, 881–894.
- 66 T. Kato, M. Oobatake, K. Machida and S. Hayashi, *Mol. Phys.*, 1992, **77**, 177–192.
- 67 S. S. Wesolowski, J. T. Fermann, T. D. Crawford and H. F. S. II, *J. Chem. Phys.*, 1997, **106**, 7178–7184.
- 68 E. L. Varetto and G. C. Pimentel, *J. Chem. Phys.*, 1971, **55**, 3813.
- 69 F. Bolduan and H. J. Jodl, *Chem. Phys. Lett.*, 1982, **85**, 283–286.
- 70 D. E. Tevault and L. Andrews, *Spectrochim. Acta, Part A*, 1974, **30**, 969.
- 71 C. H. Bibart and G. E. Ewing, *J. Chem. Phys.*, 1974, **61**, 1284–1292.
- 72 D. Luckhaus and M. Quack, *Chem. Phys. Lett.*, 1992, **199**, 293–301.
- 73 Y. Dimitrova, *Spectrochim. Acta, Part A*, 2004, **60**, 1–8.
- 74 K. J. Feierabend, D. K. Havey, M. E. Varner, J. F. Stanton and V. Vaida, *J. Chem. Phys.*, 2006, **124**, 124323.
- 75 H. G. Kjaergaard, *J. Phys. Chem. A*, 2002, **106**, 2979–2987.
- 76 K. Uzi, *Chem. Phys. Lett.*, 1990, **170**, 17–20.
- 77 T. Schimanouchi, *Tables of Molecular Vibrational Frequencies, Part 5*, NSRDS-NBS 39, 1972.
- 78 S. Y. Venyaminov and F. G. Prendergast, *Anal. Biochem.*, 1997, **248**, 234–245.
- 79 Y. Dimitrova, *Spectrochim. Acta, Part A*, 2003, **59**, 1919–1927.
- 80 D. Forney, W. E. Thompson and M. E. Jacox, *J. Chem. Phys.*, 1993, **99**, 7393.
- 81 D. B. Chesnut and A. L. Crumbliss, *Chem. Phys.*, 2005, **315**, 53–58.
- 82 M. W. Chase, *NIST-JANAF Thermochemical Tables*, American Chemical Society, American Institute of Physics for the National Institute of Standards and Technology, Washington, DC, 1998.
- 83 D. Sporleder and G. E. Ewing, *J. Phys. Chem. A*, 2001, **105**, 1838–1846.
- 84 K. C. Thompson and P. Margey, *Phys. Chem. Chem. Phys.*, 2003, **5**, 2970–2975.
- 85 K. Y. Lee, C. Amatore and J. K. Kochi, *J. Phys. Chem.*, 1991, **95**, 1285–1294.
- 86 E. Bosch and J. K. Kochi, *J. Org. Chem.*, 1994, **59**, 3314–3325.
- 87 D. J. Millen and D. Watson, *J. Chem. Soc.*, 1957, 1369–1372.
- 88 J. E. Harrar, L. P. Rigdon and S. F. Rice, *J. Raman Spectrosc.*, 1997, **28**, 891–899.
- 89 B. Lam, M. L. Diamond, A. J. Simpson, P. A. Makar, J. Truong and N. A. Hernandez-Martinez, *Atmos. Environ.*, 2005, **35**, 6578–6586.
- 90 S. P. Sander, A. R. Ravishankara, R. R. Friedl, D. M. Golden, C. E. Kolb, M. J. Kurylo, M. J. Molina, G. K. Moortgat, B. J. Finlayson-Pitts, P. H. Wine, R. E. Huie and V. L. Orkin, *Chemical Kinetics and Photochemical Data for Use in Atmospheric Studies. Evaluation Number 15 JPL Publication 06-2*, National Aeronautics and Space Administration, Jet Propulsion Laboratory, Pasadena, CA, 2006.
- 91 C. C. Addison, *Chem. Rev.*, 1980, **80**, 21–39.
- 92 T. F. Redmond and B. B. Wayland, *J. Phys. Chem.*, 1968, **72**, 1626–1629.
- 93 J. N. Pitts, E. Sanhueza, R. Atkinson, W. P. L. Carter, A. M. Winer, G. W. Harris and C. N. Plum, *Int. J. Chem. Kinet.*, 1984, **16**, 919–939.
- 94 J. N. Pitts, Jr, T. J. Wallington, H. W. Biermann and A. M. Winer, *Atmos. Environ.*, 1985, **19**, 763–767.
- 95 A. Febo and C. Perrino, *Atmos. Environ., Part A*, 1991, **25**, 1055–1061.
- 96 F. Sakamaki, S. Hatakeyama and H. Akimoto, *Int. J. Chem. Kinet.*, 1983, **15**, 1013–1029.
- 97 R. Svensson, E. Ljungstrom and O. Lindqvist, *Atmos. Environ.*, 1987, **21**, 1529–1539.
- 98 M. E. Jenkin, R. A. Cox and D. J. Williams, *Atmos. Environ.*, 1988, **22**, 487–498.
- 99 P. Wiesen, J. Kleffmann, R. Kurtenbach and K. H. Becker, *Faraday Discuss.*, 1995, **100**, 121–127.
- 100 R. M. Harrison and G. M. Collins, *J. Atmos. Chem.*, 1998, **30**, 397–406.
- 101 M. H. Harwood and R. L. Jones, *J. Geophys. Res., [Atmos.]*, 1994, **99**, 22955–22964.
- 102 I. C. Hisatsune, *J. Phys. Chem.*, 1961, **65**, 2249–2253.
- 103 G. Inoue, Y. Nakata, Y. Usui, H. Akimoto and M. Okuda, *J. Chem. Phys.*, 1979, **70**, 3689–3693.
- 104 R. Atkinson, D. L. Baulch, R. A. Cox, J. N. Crowley, R. F. Hampson, R. G. Hynes, M. E. Jenkin, M. J. Rossi and J. Troe, *Atmos. Chem. Phys.*, 2004, **4**, 1461–1738.
- 105 F. M. Tao, K. Higgins, W. Klemperer and D. D. Nelson, *Geophys. Res. Lett.*, 1996, **23**, 1797–1800.
- 106 A. S. Pimentel, F. C. A. Lima and A. B. F. d. Silva, *J. Phys. Chem. A*, 2007, **111**, 2913–2920.
- 107 D. A. Syomin and B. J. Finlayson-Pitts, *Phys. Chem. Chem. Phys.*, 2003, **5**, 5236–5242.
- 108 J. Stutz, B. Alicke, R. Ackermann, A. Geyer, S. H. Wang, A. B. White, E. J. Williams, C. W. Spicer and J. D. Fast, *J. Geophys. Res., [Atmos.]*, 2004, **109**.